Formation of Disk Galaxies: Warm Dark Matter and the Angular Momentum problem

Jesper Sommer-Larsen and Alexandre Dolgov
Theoretical Astrophysics Center, Juliane Maries Vej 30, DK-2100 Copenhagen Ø, Denmark

ABSTRACT

We have performed TreeSPH simulations of disk galaxy formation in various warm dark matter (WDM) cosmologies. Our results indicate that for a range of WDM free-streaming masses, the disk galaxy formation angular momentum problem can be *completely* resolved by going to the WDM structure formation scenario, without having to invoke stellar feedback processes at all. We also confirm our previous suspicion, that part of the angular momentum problem is due to numerical effects, most likely related to the shock capturing, artificial viscosity used in SPH. Furthermore we find that we can match the observed I-band Tully-Fisher (TF) relation, provided that the mass-to-light ratio of disk galaxies is $(M/L_I) \simeq 0.8$. We argue that this is quite a reasonable value in comparison with various dynamical and spectrophotometric estimates, including one given in this paper. We speculate that our success in matching the TF relation may be due to WDM halos being less centrally concentrated than CDM halos and suggest to check this exciting possibility with high resolution simulations, in particular in low Ω_M, WDM cosmologies. Finally, we discuss possible physical candidates for WDM particles extensively. We find that the most promising are neutrinos with weaker or stronger interactions than normal, majorons (light pseudogoldstone bosons) or mirror or shadow world neutrinos.

Subject headings: cosmology: theory — dark matter — galaxies: formation — galaxies: structure — elementary particles — methods: numerical

1. Introduction

The formation of galactic disks is one of the most important unsolved problems in astrophysics today. In the currently favored hierarchical clustering framework, disks form in the potential wells of dark matter halos as the baryonic material cools and collapses dissipatively. It has been shown (Fall & Efstathiou 1980) that disks formed in this way

can be expected to possess the observed amount of angular momentum (and therefore the observed spatial extent for a given mass and profile shape), but only under the condition that the infalling gas retain most of its original angular momentum.

Numerical simulations of this collapse scenario in the cold dark matter cosmological context (e.g., Navarro & Benz 1991, Navarro & White 1994, Navarro, Frenk, & White 1995), however, have so far consistently indicated that when only cooling processes are included the infalling gas loses too much angular momentum (by over an order of magnitude) and the resulting disks are accordingly much smaller than required by the observations. This discrepancy is known as the *angular momentum problem* of disk galaxy formation. It arises from the combination of the following two facts: a) In the CDM scenario the magnitude of linear density fluctuations $\sigma(M) =< (\delta M/M)^2 >^{1/2}$ increases steadily with decreasing mass scale M leading to the formation of non-linear, virialized structures at increasingly early epochs with decreasing mass i.e. the hierarchical "bottom-up" scenario. b) Gas cooling is very efficient at early times due to gas densities being generally higher at high redshift as well as the rate of inverse Compton cooling also increasing very rapidly with redshift ($\propto (1+z)^4$). a) and b) together lead to rapid condensation of small, dense gas clouds, which subsequently lose energy and (orbital) angular momentum by dynamical friction against the surrounding dark matter halo before they eventually merge to form the central disk. A mechanism is therefore needed that prevents, or at least delays, the collapse of protogalactic gas clouds and allows the gas to preserve a larger fraction of its angular momentum as it settles into the disk. (Such a mechanism is also helpful in solving the *overcooling problem*, namely the observation (White & Rees 1978) that cooling is expected to be so efficient at early times that most of the gas should have been converted to stars well before the assembly of present-day galactic disks). Weil, Eke, & Efstathiou (1998) have shown that if the early cooling is suppressed (by whatever means), numerical simulations can indeed yield more realistically sized disks - see also Eke, Efstathiou & Wright (1999). The physical mechanism by which cooling is suppressed or counteracted, however, was not specified.

Sommer-Larsen et al. (1999, hereafter SLGV99) discussed the effects of various stellar reheating mechanisms in more detail using numerical TreeSPH simulations of disk galaxy formation in a CDM cosmological context. They found that more or less uniform reheating of the Universe resulting from a putative early epoch of population III star formation ($z \gtrsim 6$) does not lead to a solution to the angular momentum problem, but that localized star-bursts in protogalactic gas clouds might: *If* the star-bursts can blow the remaining, bulk part of the gas out of the small and dense dark matter halos of the clouds, then the test simulations of SLGV99 show that the gas later gradually settles forming an extended, high angular momentum disk galaxy in the central parts of a large, common dark matter halo. The physics of global gas blow-out processes were considered in early calculations by Dekel

& Silk (1986) and Yoshii & Arimoto (1987) indicating that star-bursts might well blow out most of the gas in small galaxies with characteristic circular speed (where the rotation curve is approximately constant) $V_c \lesssim 100$ km/s. Unfortunately, more recent, detailed simulations by Mac Low & Ferrara (1999) suggest that this global blow-out scenario may not work so well, even in small (disk) galaxies: The star-bursts typically lead to bipolar outflows of very hot gas perpendicular to the disk of the small galaxy, only expelling a minor fraction of the disk gas.

Moreover, various possible shortcomings of the CDM cosmological scenario in relation to structure formation on galactic scales have recently been discussed in the literature: 1) CDM possibly leads to the formation of too many small galaxies relative to what is observed, i.e. the *missing satellites problem* (e.g., Klypin et al. 1999). 2) Even if galactic winds due to star-bursts can significantly reduce the number of visible dwarf galaxies formed, sufficiently many of the small and tightly bound dark matter systems left behind can still survive to the present day in the dark matter halos of larger galaxies like the Milky Way to possibly destroy the large, central disks via gravitational heating, as discussed by Moore et al. 1999a. 3) The dark matter halos produced in CDM cosmological simulations tend to have central cusps with $\rho_{DM}(r) \propto r^{-N}, N \sim 1-2$ (Dubinski & Carlberg 1991, Navarro et al. 1996, Fukushige & Makino 1997, Moore et al. 1998, Kravtsov et al. 1998, Gelato & Sommer-Larsen 1999). This is in disagreement with the flat, central dark matter density profiles (cores) inferred from observations of the kinematics of dwarf and low surface brightness galaxies (e.g., Burkert 1995, de Blok & McGaugh 1997, Kravtsov et al. 1998, Moore et al. 1999b, but see also van den Bosch et al. 1999).

The first two problems may possibly be overcome by invoking warm dark matter (WDM) instead of CDM: WDM is similar to CDM on mass scales larger than the free-streaming mass $M_{f,WDM} \sim 10^{10}$-10^{12} $M_\odot$, but density fluctuations $\sigma_{WDM}(M)$ are suppressed on mass scales $M < M_{f,WDM}$ relative to CDM (but note that they are still non-zero as $\sigma_{WDM}(M < M_{f,WDM}) \simeq \sigma_{WDM}(M_{f,WDM})$ - see section 2). As a consequence, fewer low mass galaxies (or "satellites") are formed cf., e.g., Moore et al. (1999a) and section 2 of this paper. The central cusps problem may be more generic cf. Huss et al. (1999) and Moore et al. (1999b), but the WDM scenario deserves further attention also on this point.

In this paper we show that the disk galaxy formation angular momentum problem most likely can be completely overcome by invoking the WDM rather than the CDM structure formation scenario and this without having to appeal to stellar feedback processes at all!

In section 2 WDM and its relation to galaxy formation is briefly discussed. Section 3 gives a short presentation of the numerical code and the initial conditions. The simulations

themselves are described in section 4, and the results are analyzed in section 5. In section 6 we discuss possible physical candidates for WDM particles extensively and in section 7 we present a final discussion and summarize our conclusions.

2. Warm Dark Matter

In this section we give a brief introduction to "conventional" warm dark matter following the approach of Bardeen et al. (1986) and using expressions from that work. We defer a much more detailed and general discussion of the relevant particle physics to section 6.

At low redshift warm dark matter particles behave in many respects in the same way as cold dark matter (see below), but from a particle physics point of view they are quite different, however: CDM particles (apart from axions) are thought to be very massive, normally with $m \gtrsim 1$ GeV, and to be non-relativistic when they decouple from the rest of the particles in the Universe at high redshift. WDM is particles with typical masses $m \sim 1$ keV, which in conventional theory decouple at high redshifts $z_{dec} \gtrsim 10^{13}$ (or $T_{dec} \gtrsim 1$ GeV) being still ultra-relativistic. At $z_{nr} \sim 10^6$-10^7 the WDM particles become non-relativistic: $3kT_{WDM} \simeq m_{WDM}c^2$. The Universe is still radiation dominated at this stage, as $z_{nr} >> z_{eq} \sim 10^4$, where z_{eq} is the redshift of matter-radiation equivalence. The horizon mass of WDM at z_{nr} defines a characteristic mass scale called the free-streaming mass $M_{f,WDM} \sim M_{H,WDM}(z_{nr})$. Pertubations on mass scales $M \lesssim M_{f,WDM}$ are damped relative to CDM due to relativistic free-streaming of the WDM particles at $z > z_{nr}$. On larger mass scales $M \gtrsim M_{f,WDM}$ WDM behaves like CDM.

Following Bardeen et al. (1986) the power spectrum of WDM (adiabatic fluctuations) can be expressed as

$$P_{WDM}(k) = T^2_{WDM}(k)\ P_{CDM}(k) \quad , \tag{1}$$

where the CDM to WDM "transfer function" can be approximated well by

$$T_{WDM}(k) = \exp\left[-\frac{kR_{f,WDM}}{2} - \frac{(kR_{f,WDM})^2}{2}\right] \tag{2}$$

and $P_{CDM}(k)$ is the CDM power spectrum for which we use the standard SCDM form. The function T^2_{WDM} is shown in Figure 1. The comoving, free-streaming scale $R_{f,WDM}$ is given by

$$R_{f,WDM} = 0.2\ \left(\frac{g_{WDM,dec}}{100}\right)^{-4/3}\ (\Omega_{WDM}h^2)^{-1}\ \mathrm{Mpc} \quad , \tag{3}$$

$g_{WDM,dec}$ being the effective number of particle degrees of freedom when the WDM particles decouple. $\Omega_{WDM}h^2$ is related to the mass of the WDM particles by

$$\Omega_{WDM}h^2 = 1.0 \left(\frac{g_{WDM,dec}}{100}\right)^{-1} \left(\frac{m_{WDM}}{\mathrm{keV}}\right) \tag{4}$$

For justification of equations (3) and (4), see section 6.

A characteristic free-streaming wave number $k_{f,WDM}$ can be defined as the k for which T^2_{WDM}=0.5. From Figure 1 it then follows that $k_{f,WDM} \times R_{f,WDM} \simeq 0.46$, so we define $k_{f,WDM} \equiv R_{f,WDM}/0.46$. Using this we can then define a characteristic free-streaming mass in terms of $\lambda_{f,WDM} \equiv 2\pi/k_{f,WDM}$ by

$$M_{f,WDM} \equiv \frac{4\pi}{3}\ \rho_{crit}\ \Omega_{WDM} \left(\frac{\lambda_{f,WDM}}{2}\right)^3 = 3.7 \cdot 10^{11}\ h^{-1}\ \Omega_{WDM} \left(\frac{R_{f,WDM}}{0.1h^{-1}\mathrm{Mpc}}\right)^3\ \mathrm{M}_\odot \tag{5}$$

Using equations (3)-(5) we can finally express the WDM particle mass in terms of this free-streaming mass

$$m_{WDM} = 2.4\ h^{5/4}\ \Omega^{1/2}_{WDM} \left(\frac{M_{f,WDM}}{10^{11}h^{-1}M_\odot}\right)^{-1/4}\ \mathrm{keV}\ \ . \tag{6}$$

The average relative mass fluctuations on mass scale M, $\sigma(M)$, can be calculated from the power spectrum $P(k)$ in linear theory as

$$\sigma^2(M) = \ < \left(\frac{\delta M}{M}\right)^2 > \ = \ \frac{1}{(2\pi)^3} \int d^3k\ P(k)\ W(kx)\ \ , \tag{7}$$

where the weight function

$$W(y) = \frac{9}{y^6}[\sin y - y\cos y]^2\ , \quad y = kx \tag{8}$$

is the square of the Fourier transform of a spherical top-hat filter of radius x (following Peebles 1980). To illustrate the difference between CDM and WDM we show in Figure 2 $\sigma(M; z = 0)$ for CDM as well as WDM with $R_{f,WDM} = 0.037$, 0.075 and 0.15 h^{-1}Mpc corresponding to free-streaming masses of 1.9×10^{10}, 1.5×10^{11} and 1.2×10^{12} $h^{-1}\mathrm{M}_\odot$ The curves have been normalized such that $\sigma_8 = 0.5$, where σ_8 is the present day value of $\sigma(M)$ defined above for M equal to the average mass within spheres of comoving radius $8h^{-1}$ Mpc.

The fact that the $\sigma(M; z = 0)$ curves flatten at low masses for WDM does *not* mean that no low mass galaxies are formed (see also Schaeffer & Silk 1988). To illustrate this we calculate the present day ($z = 0$) mass spectrum using (linear) Press-Schechter (PS) theory:

The mass spectrum $dN(M)/dM$ in the linear PS approximation is given by (e.g. White 1993)

$$\frac{dN(M)}{dM}(z=0) = -\sqrt{\frac{2}{\pi}}\frac{\bar{\rho}}{M}\frac{\delta_c}{\sigma^2(M;z=0)}\frac{d\sigma(M;z=0)}{dM}\exp\left[\frac{-\delta_c^2}{2\sigma^2(M;z=0)}\right] \quad , \qquad (9)$$

where we take $\delta_c = 1.69$ (see White 1993). The mass spectra obtained in this way for CDM and the WDM described above are shown in Figure 3. Clearly, for WDM dN/dM still decreases with M as for CDM, but, for example, for masses three orders of magnitude below the free-streaming mass dN/dM is down by more than an order of magnitude relative to CDM, whereas for masses of the order of or larger than the free-streaming mass dN/dM is essentially the same for WDM and CDM. We caution, however, that the PS theory applied above is not completely rigorous and hence that N-body WDM simulations should be undertaken to determine WDM mass spectra more properly.

3. The code and the initial conditions

3.1. The code

We use the gridless Lagrangian N-body and Smoothed Particle Hydrodynamics code TreeSPH described in SLGV99. Our TreeSPH code is modeled after that of Hernquist & Katz (1989).

We include gas cooling and heating terms as in Vedel et al. (1994). The heating corresponds to a redshift-dependent, homogeneous and isotropic UVX background field. We assume a rather hard (spectral index -1) quasar like field

$$J_\nu(z) = J_{-21}(z) \times 10^{-21}\left(\frac{\nu}{\nu_L}\right)^{-1} \mathrm{erg\,cm^{-2}\,sr^{-1}\,Hz^{-1}\,s^{-1}}, \qquad (10)$$

where ν_L is the Lyman limit frequency, with the redshift-dependent normalization

$$J_{-21}(z) = \frac{10}{1+[5/(1+z)]^4} \qquad (11)$$

of Efstathiou (1992). For greater realism one could build on the detailed study of Haardt & Madau (1996), but our adopted background field is quantitatively not too dissimilar from theirs (once allowance is made for our simplified spectral shape), at least at redshifts $z \lesssim 3$, and should be adequate for the level of detail we can represent in the simulations. The code furthermore incorporates inverse Compton cooling, which is also explicitly redshift-dependent.

SLGV99 studied the effects of star-formation in terms of the subsequent energy and momentum feedback processes to the gas as a means of resolving the angular momentum problem of disk galaxy formation. In this paper we study the effects of going from CDM to WDM, as an alternative. In order to separate the various effects clearly we describe in this paper what in SLGV99 was dubbed "passive" simulations, i.e. simulations with no star-formation and feedback effects.

The smoothing length of each SPH particle is adjusted so as to keep the number of neighbors close to 50.

3.2. The initial conditions

Our cosmological initial conditions are based on a standard ($\Omega = 1$, $\Lambda = 0$) CDM model with Hubble constant $H_0 = 100h\,\mathrm{km\,s^{-1}\,Mpc^{-1}} = 50\,\mathrm{km\,s^{-1}\,Mpc^{-1}}$. On the scales of interest to us the effective index of the power spectrum is approximately -2 ($P(k) \propto k^{-2}$). Following Eke, Cole, & Frenk (1996) we normalize the spectrum to $\sigma_8(z = 0) = 0.5$, where as customary σ_8^2 is the mass variance within spheres of comoving radius $8h^{-1}$ Mpc, extrapolated from the linear regime of perturbation growth.

We begin by performing a large-scale simulation within a sphere of comoving radius 40 Mpc. Individual halos are then selected from the final state and sampled at higher resolution. The original large-scale simulation is used to provide a tidal field acting on the resampled halos, which are evolved separately in a second round of simulations.

Approximately 2.5×10^5 particles are initially placed on a cubic lattice within the large sphere. Position and velocity perturbations are then applied according to the Zel'dovich (1970) approximation. The perturbations consist of the superposition of $N_k \sim 4 \times 10^4$ plane waves sampling a Gaussian random field with variance given by the power spectrum. Following Navarro & White (1994) we use an equal number of waves per logarithmic interval in k-space. The phases of these waves are random and only wavenumbers between the fundamental and Nyquist wavenumber of the lattice are included. The initial redshift (which determines the amplitude of the initial perturbations) is $z_i \simeq 18$.

The evolution of this system to $z = 0$ is then computed using a tree code. Only gravitational forces are included in this first simulation. In the final state we identify four virialized, isolated halos with circular velocities between 200 and 260 $\mathrm{km\,s^{-1}}$ in the innermost 20 Mpc of the simulation. We expect that a significant fraction of such halos should host disk galaxies similar to the Milky Way since the circular velocities are in the same range and our halos were chosen to lie "in the field", away from larger concentrations

of mass. We adopt the customary working definition of the virial radius as the radius r_{200} of a sphere enclosing a mean density of 200 times the critical cosmic value. Tracing the particles in these halos back to the initial conditions, we find that they all come from regions that fit within spheres of comoving radius ~ 3 Mpc.

Each of these spheres at $z \simeq 18$ is then resampled with a lattice 4 times finer in each spatial dimension in our moderate resolution (MR) simulations and 8 times finer in our high resolution (HR) simulations. Each sphere contains about 7000 points of this new lattice in our MR simulations and about 56000 points in our HR simulations. We assign one dark matter (DM) particle and two SPH particles to each of these points for the MR simulations and one DM particle and one SPH particle to each point for the HR simulations. The SPH particles are positioned at random within one gas gravitational softening length (see below) of their parent DM particle. Note that at this redshift the DM particles are spaced by about 14 kpc for the MR simulations and 7 kpc for the HR simulations, so that each SPH particle is rather closely associated with its parent DM particle. Table 1 lists the precise number of SPH and DM particles in each sphere. We generally use a baryonic mass fraction $\Omega_b = 0.05$, consistent with nucleosynthesis constraints ($0.01h^{-2} \lesssim \Omega_b \lesssim 0.02h^{-2}$), but use $\Omega_b = 0.10$, which is more consistent with the observationally determined baryonic fractions in galaxy groups and clusters, in some of the MR simulations. This leads to masses of $1.1 \times 10^9\, M_\odot$ for the DM and $2.9 \times 10^7\, M_\odot$ for the SPH particles for the MR simulations with $\Omega_b = 0.05$, 1.0×10^9 and $5.8 \times 10^7\ M_\odot$ respectively for the $\Omega_b = 0.10$ MR simulations and 1.4×10^8 and $7.3 \times 10^6\ M_\odot$ for the HR simulations, which all have $\Omega_b = 0.05$ The SPH particles are assigned an initial thermal energy corresponding to a temperature $T_i \simeq 100$ K. In order to include small-scale power that could not be sampled in the first simulation, we add shorter-wavelength plane waves in a way that preserves an equal number of waves per interval in $\log k$. Given the variety of properties of the WDM particle candidates discussed in section 6 and that the purpose of this paper is to investigate qualitatively the effects on disk galaxy formation of going from CDM to WDM we approximate $T_{WDM}(k)$ by a step function

$$\tilde{T}_{WDM}(k) = \begin{cases} 1 & k \leq k_c\ , \\ 0 & k > k_c\ . \end{cases} \tag{12}$$

We find that for a given $R_{f,WDM}$, $\tilde{T}_{WDM}(k)$, with $k_c = 0.46 R_{f,WDM}^{-1}$ (cf. section 2), gives a reasonable match to $T_{WDM}(k)$ as shown in Figure 1 (dotted line). In Figure 2 we show by the thin solid line $\tilde{\sigma}(M; z = 0)$ for $k_c = 6.2\ h$ Mpc^{-1} (corresponding to $R_{f,WDM} \simeq 0.075\ h^{-1}$Mpc). As can be seen from the figure, the match to $\sigma(M; z = 0)$ for $R_{f,WDM} = 0.075\ h^{-1}$Mpc is also reasonably good. The WDM simulations described in this paper are hence performed using the original, standard CDM power spectrum used in

SLGV99, modified to WDM by

$$\tilde{T}_{WDM}(k) = \begin{cases} 1 & kR_{f,WDM} \leq 0.46 \ , \\ 0 & kR_{f,WDM} > 0.46 \ . \end{cases} \tag{13}$$

In this spirit we are also able to reuse the original, background CDM cosmological simulation for the WDM simulations presented in this work, as the typical WDM wavenumbers k_c used here are comparable to the Nyquist wavenumber of the CDM cosmological simulation.

We use stored intermediate results from the large cosmological simulation to provide a time-dependent tidal field acting on the resampled spheres. This is achieved by treating the original particles outside the resampled sphere as passive, interpolating their positions between successive snapshots of the original simulation and incorporating them into the particle tree that the code constructs on each step for the evaluation of gravitational forces. Gravitational interactions between particles are softened according to the prescription of Hernquist & Katz (1989), with softening lengths of 3 kpc for the gas particles and 10 kpc for the dark matter particles in the MR simulations, 1.5 and 5 kpc, respectively, in the HR simulations, and 40 kpc for the "passive" dark matter particles that provide the tidal field from the original large-scale simulation. The gravitational softening lengths are kept constant in physical units throughout the evolution of the system.

4. The simulations

For the WDM galaxy formation simulations we identify the four resampling spheres S1-S4, also used by SLGV99 for their CDM galaxy formation simulations.

It seems reasonable to assume that $M_{f,WDM} \gtrsim 10^9 - 10^{10} M_\odot$ in order for a change from CDM to WDM to have a significant impact on the disk galaxy formation angular momentum problem as well as the other possible CDM problems listed in section 1. On the other hand, if $M_{f,WDM} \gtrsim 10^{13} M_\odot$ the bulk of galaxy and star formation will likely take place too late relative to the observed star-formation history of the Universe, as discussed below. Consequently we initially carry out three MR simulations (with $\Omega_b = 0.05$) of the formation of disk galaxy S4 with $k_c = 12.4$, 6.2 and 3.1 h Mpc^{-1} corresponding to free-streaming masses of 1.9×10^{10}, 1.5×10^{11} and 1.2×10^{12} $h^{-1} M_\odot$ by eqs. (5) and (13). We denote warm dark matter with these characteristics WDM1, WDM2 and WDM3 in the following and the corresponding simulations runs #1-3. Figure 4 shows the specific angular momentum j_{disk} (upper panel) and cooled out gas mass M_{disk} (lower panel) of the central, cold and dense, forming disk (with $R \leq 30$ kpc and $n_H > 0.01$ cm^{-3}) as a function of time since Big Bang (at times when central merging is in process, i.e. when a merging

satellite is inside of $r = 30$ kpc, j_{disk} and M_{disk} are not shown in this and the following figures. Such merging episodes are clearly seen in the figures as steep increases in $M_{disk}(t)$). The observed value of j for Milky Way sized disk galaxies is $j_{obs} \sim$ 1000-1500 kpc km/s - see section 5. As can be seen from Figure 4, the CDM and WDM3 simulations generally have $j \lesssim 200$ kpc km/s. Moreover, for the WDM3 simulations cold, dense gas, and hence the basis for star formation, is not formed before $t \sim 4.5$ Gyr, corresponding to a redshift $z \sim 1$, in disagreement with the observed star-formation history of the Universe - see, e.g., Madau et al. (1996) and Steidel et al. (1999). The WDM1 and WDM2 simulations look much more promising, both having $j \gtrsim 400$ kpc km/s and for WDM2 even $j > 800$ kpc km/s at present (z=0). Moreover, for the WDM1 and WDM2 simulations, gas cools out approximately as early and at the same rate as for the CDM simulation.

Guided by the results above we secondly carry out three MR WDM2 simulations (with $\Omega_b = 0.05$) of the formation of the disk galaxies S1-S3 (runs #4-6). As discussed in SLGV99 one may expect that part of the angular momentum problem is related to numerical effects, in particular angular momentum transport due to artificial viscosity. One would expect this effect to be reduced as the resolution of the simulations is increased. Consequently, we thirdly carry out four WDM2 HR simulations (with $\Omega_b = 0.05$) of galaxies S1-S4 with 8 times the mass resolution (4 times for SPH) of the MR simulations (runs #7-10).

The effects of a background UVX radiation field on disk galaxy formation has been discussed by, e.g., Vedel et al. (1994) and Navarro & Steinmetz (1997). To study the effect of not including a UVX field in the simulations (but still inverse Compton cooling) we fourthly carry out four MR WDM2 simulations (with $\Omega_b = 0.05$) of galaxies S1-S4 without a UVX field (runs #11-14). Finally, to study the effect of having a baryonic fraction of 0.10 rather than 0.05 we carry out four MR WDM2 simulations of galaxies S1-S4 with $\Omega_b = 0.10$ and with a background UVX radiation field (runs #15-18).

Parameters for all the simulations are listed in Table 1.

5. Results

5.1. Disk masses and specific angular momenta

Table 2 presents some global properties of the final collapsed objects in our 18 simulations. The first column is the simulation label, as described in the previous section. Columns 2, 3, and 4 respectively hold the virial mass M_{200}, the virial radius r_{200}, and the circular velocity V_{200} at the virial radius. The numbers $N_{\rm gas}$ and $N_{\rm DM}$ of gas and DM particles inside the virial radius are in columns 5 and 6, and the corresponding masses $M_{\rm gas}$

and $M_{\rm DM}$ in columns 7 and 8. Columns 9, 10, and 11 show the number of gas particles $N_{\rm disk}$, the corresponding baryonic mass $M_{\rm disk}$, and the ratio $M_{\rm disk}/\Omega_b M_{200}$ for the cold disk present at the end of each simulation.

The time evolution of j_{disk} and M_{disk} for the WDM2 MR simulations with Ω_b=0.05 of the forming disk galaxies S1-S4 is shown in Figures 5-8 together with those of the corresponding "passive" CDM simulations (from SLGV99) and of the WDM2 HR simulations of galaxies S1-S4 (though not j_{disk} for galaxy S1 - see below). The WDM2 simulations are clearly producing disks with considerably larger j_{disk} than the CDM simulations, whereas the growth of disk mass M_{disk} is fairly similar for the two types of dark matter. Comparing the WDM2 MR and HR simulations qualitative agreement is found in the j_{disk} and M_{disk} evolution between the two types of simulations. This is gratifying, since the substructure in the forming galaxies with this kind of dark matter in general is resolved even in the MR simulations (with one exception, as discussed below). For any given galaxy, however, $j_{disk}(t)$ for the HR simulations generally exceeds j_{disk} for the MR simulations. This is particularly evident towards the end of the simulations ($z \sim 0$), where the ratio of the two typically is 1.5-2.5. This confirms the suspicion of SLGV99, that part of the angular momentum problem is due to numerical effects, most likely related to spurious angular momentum transport due to the shock capturing artificial viscosity used in SPH (we have performed idealized tests which indicate that going from the standard Monaghan-Gingold viscosity (Monaghan & Gingold 1983) used in this work to the shear-free Balsara (1995) viscosity does not result in higher specific angular momentum disks at a given level of resolution - see also the discussion in SLGV99).

Galaxy S1 is very different from the others: At about $t \sim 4$ Gyrs the central galaxy develops into a kinematically complex system through accretion of counterrotating hot gas and a cold gas merging event. By then it consists of an inner, high density disk surrounded by an outer, more extended but lower density counterrotating disk. In the MR simulations the spin vector of the inner disk flips around and aligns itself with that of the outer disk during the next 2-4 Gyrs. In contrast, the inner disk in the HR simulation does not "flip" relative to the outer during the remaining $\sim$ 9 Gyrs of the simulation. This clearly indicates that the gasdynamical (and perhaps also gravitational) resolution is not sufficient to resolve the long-lived, discontinuous kinematics. We chose to plot and give values for the specific angular momenta of the final disks formed in the MR simulations of galaxy S1, as these disks are kinematically relaxed. But given the possible resolution problems in these simulations, we do not use the results in any of the following quantitative estimates of the angular momentum properties of disks formed in WDM simulations. We do not give specific angular momenta results for the HR simulation of galaxy S1, as this system is kinematically unrelaxed during most of the simulation, including the final state. Given the observational

variety of galaxies, including some with counterrotating disks (e.g., Thakar & Ryden 1998 and references therein), we find it almost reassuring that not *all* simulated galaxies end up as extended, kinematically coherent disks, as long as most do!

The time evolution of j_{disk} and M_{disk} of galaxies S1-S4 for the WDM2 MR simulations with Ω_b=0.05 and no UVX background radiation field is shown in Figure 9 (runs #11-14). Not surprisingly, the final disk masses are somewhat larger (on average by about 25%) than for the corresponding runs with a UVX field. This is due to the somewhat more efficient radiative cooling and lack of photo-heating in the absence of a UVX field. Moreover, the specific angular momenta of the final disks are on average about 45% larger than for the runs with a UVX field - we comment on this below.

Finally, the time evolution of j_{disk} and M_{disk} of galaxies S1-S4 for the WDM2 MR simulations with Ω_b=0.10 and a UVX field is shown in Figure 10 (runs #15-18). The final disk masses are about a factor of 2.5 times those of the corresponding Ω_b=0.05 runs. This is not far from the factor of about $2^{3/2}$ expected from cooling flow theory assuming an isothermal dark matter potential (Sommer-Larsen 1991). The specific angular momenta of the final disks are about a factor 2.8 times those of the corresponding Ω_b=0.05 runs.

In order to compare the masses and specific angular momenta of the final disks to observations a characteristic circular velocity, V_c, is assigned to the model disk galaxies in the following way: Courteau (1997) compared for Tully-Fisher applications optical rotation curves with 21 cm linewidths of disk galaxies. He found from the data that the circular velocity, $V_{2.2}$, at 2.2 exponential disk scale-lengths from the center (where the circular velocity of the disk alone peaks) gives the best match to the 21 cm linewidths. Since the disks of our model galaxies are not perfectly exponential and generally still somewhat too concentrated compared to observations we determine $V_c = V_{2.2}$ iteratively. Given the dark matter part of the rotation curve and the disk mass, both taken from the simulations, and using the observational relation between the median exponential disk scale-length and the characteristic circular velocity

$$\bar{R}_d = 1.9\ h^{-1}\ \left(\frac{V_c}{200\ \mathrm{km/s}}\right)^{1.05}\ \ \mathrm{kpc} \tag{14}$$

(SLGV99), $V_c = V_{2.2}$ is determined in the following way: Starting from an initially adopted $V_{2.2}$ ($= V_c$) the corresponding characteristic scale-length is determined using (14). Assuming that the "real" disk is exponential and given the disk mass M_{disk} and scale-length R_d the disk part of the rotation curve is determined. This is then added in quadrature to the dark matter part of the rotation curve and finally $V_{2.2}$ is determined from the combined rotation curve. This value is then used as input to the above procedure, which is repeated until the input $V_{2.2}$ equals the output $V_{2.2}$.

As the baryonic mass is somewhat more centrally concentrated than the exponential disk of the same mass the dark matter halo may be somewhat too "pinched". This means that $V_c = V_{2.2}$ determined in this way actually is an upper limit in this connection. We estimate, however, that the effect of the extra pinching is quite small: As an example we show in Figure 11 the dark matter part of the rotation curve $V_{c,DM}(R)$ (upper panel) and $M_{disk}(R)$ (lower panel) for the four simulations runs #4, 7, 11 and 15 of galaxy S1 at z=0. As can be seen from the Figure, the final dark matter halo rotation curves are fairly insensitive to the quite different amounts of baryonic mass inside of $R_{2.2} \simeq$ 10-15 kpc for h=0.5. Another possible concern is that part of the cooled-out mass may end up in a central component/bulge, which may change the estimate of $V_{2.2}$. Assuming that no more than 20% of the baryonic mass is in such a component for Sb-Sd galaxies (see section 5.2) we find, however, that this leads to an average increase of $V_{2.2}$ of no more than about 1%, so we neglect this effect as well. Finally, for the arguments given in this paper, we can neglect the effects of a possible truncation of the disk at $\sim 4\ R_D$ (van der Kruit & Searle 1982).

The specific angular momenta j_{disk} and iteratively determined characteristic circular velocities $V_c = V_{2.2}$ of the final disks in the 18 simulations are given in Table 3. The Table also lists our computed values for the dimensionless spin parameter $\lambda \equiv J|E|^{1/2}/GM^{5/2}$ (column 3) evaluated at the *infall radius* r_{inf} (column 5). This radius is defined by $M_{DM}(r_{inf})/(1-\Omega_b) = M_{disk}/\Omega_b$, and is of order 120-200 kpc in all our runs. It represents a characteristic radius, at the present time, of the dark matter originally associated with the amount of gas currently in the disk. In Figure 12 we show the "normalized" specific angular momenta $\tilde{j}_{disk} = j_{disk}/V_c^2$ of the final disk galaxies formed in all WDM2 runs (except run #7) as a function of V_c. As argued by SLGV99 one expects $\tilde{j}_{disk}$ to be almost independent of V_c on both theoretical and observational grounds. Also shown in the figure is the median "observed" value of $\tilde{j}_{disk}$, calculated using equation (14) and

$$\tilde{j} = \frac{j}{V_c^2} = \frac{1.68 R_d}{V_c} \tag{15}$$

(SLGV99), and the observational 1-σ and 2-σ contours.

For the MR WDM2 simulations of galaxies S2-S4 with $\Omega_b = 0.05$ and including effects of a UVX field, the median $\tilde{j}_{disk}$ is 0.61 $\pm$ 0.11 dex below the "observed" value, corresponding to a factor of 4. This is almost an order of magnitude better than what is obtained with "passive" CDM simulations - see, e.g., Navarro & Steinmetz (1997) and SLGV99.

For the HR WDM2 simulations of galaxies S2-S4 with $\Omega_b = 0.05$ and including effects of a UVX field the median $\tilde{j}_{disk}$ is (just) 0.32 $\pm$ 0.07 dex below the observed, corresponding to a factor of two. As noted above this strongly suggests that part of the angular momentum

problem is related to numerical problems.

For the MR WDM2 simulations of galaxies S2-S4 with $\Omega_b = 0.05$ and no UVX field the median $\tilde{j}_{disk}$ is 0.45 ± 0.13 dex below the observed, corresponding to a factor of 2.8. The larger specific angular momenta obtained for the final disks relative to the simulations including a UVX field are due to the more efficient cooling resulting in more high angular momentum gas from the outer regions of the halo to be deposited onto the disk during the simulations, as discussed by Navarro & Steinmetz (1997). This effect is even more pronounced in the MR WDM2 simulations with Ω_b=0.10 and a UVX field due to the ~ 4 times higher cooling rates compared to the similar simulations with Ω_b=0.05: For galaxies S2-S4 the median $\tilde{j}_{disk}$ is (just) 0.36±0.12 dex below the observed corresponding to a factor of 2.3.

Summarizing, we find that increasing the mass resolution by a factor of 8 (4 for SPH) leads to the formation of disk galaxies with final specific angular momenta, which are about a factor two larger than those of the otherwise identical medium resolution simulations and just a factor of about two smaller than those of observed disk galaxies. Moreover, the median value of the spin parameter λ for the three HR simulation galaxies S2-S4 is 0.039. Assuming a theoretical median value of λ of 0.05 (Barnes & Efstathiou 1987; Heavens & Peacock 1988) the discrepancy is further reduced to a factor of 1.6, which may very well be gained by going to even higher resolution. Furthermore we also find that going from a baryonic fraction of f_b=0.05 to f_b=0.10 (which may well be more realistic) also improves the situation considerably for the MR simulations, as discussed above. To illustrate this we show in Figure 13 a face-on view and in Figure 14 an edge-on view of the final galaxy formed in run # 18 (this has the largest specific angular momentum of all the galaxies formed, $j_{disk} \simeq 2000$ kpc km/s). Further, in Figure 15 we show the (azimuthally averaged) surface density profiles of the final disks in runs #15-18. Clearly, it is no longer a problem to form extended disks in cosmological simulations!

All in all, it seems therefore plausible that the disk galaxy angular momentum problem can be *completely* resolved by going to the WDM cosmological structure formation scenario, provided that the WDM free-streaming mass is $M_{f,WDM} \sim 10^{11} h^{-1} M_\odot$ within about a factor of three if Ω_M=1. We shall touch briefly on the $\Omega_M < 1$ case in section 7.

5.2. The Tully-Fisher relation and mass-to-light ratios of disk galaxies

In Figure 16 we show $M_{disk}(V_c)$ of the final disk galaxies formed in all 16 WDM2 runs together with the I-band Tully-Fisher relation (TF) of Giovanelli et al. (1997) for h=0.5,

converted to mass assuming mass-to-light ratios $(M/L_I) = 0.25$, 0.5 and 1.0 in solar units (used throughout). The slope of the "theoretical" TF matches that of the observed very well for a constant mass-to-light ratio. But for h=0.5 the required $(M/L_I) \simeq 0.6$, which is somewhat low. Assuming h=0.7 and that the final disk masses scale as h^{-1} (which should be a good first approximation) a $(M/L_I) \simeq 0.8$ gives a good match (see Figure 17). This value is fairly consistent with dynamical estimates of (M/L_I) for disk galaxies: Persic & Salucci (1992) find $(M/L_B) = 1.24h$ for disks, corresponding to $(M/L_B) = 0.86$ for h=0.7 or $(M/L_I) \simeq 0.6$ assuming Sbc type colours. Syer et al. (1997) find $(M/L_I) < 1.9\ h$ from disk stability arguments corresponding to $(M/L_I) < 1.3$ for h=0.7. The (M/L)s obtained from stellar population synthesis depend strongly on the assumed initial mass function (IMF), in particular the effective lower mass cut. Recent determinations of the (M/L) of disk galaxies based on what is thought to be realistic IMFs range from $(M/L_B) \simeq 1.9$ (Fukugita et al. 1998), corresponding to $(M/L_I) \simeq 1.3$, to $(M/L_I) \simeq 1.0$ for Milky Way sized disk galaxies and slightly less for smaller galaxies (Boissier & Prantzos 1999).

In summary, we find from the results of our WDM2 simulations, that we can match the observed TF relation provided $(M/L_I) \simeq 0.8$ for disk galaxies and furthermore that such a (M/L_I) is fairly compatible with dynamical as well as stellar population synthesis estimates.

Steinmetz & Navarro (1999) and Navarro & Steinmetz (1999) find a discrepancy between the observed and "theoretical" TF on the basis of GRAPESPH, SCDM and ΛCDM simulations of disk galaxy formation. This discrepancy between their work and ours is partly resolved if $(M/L_I) \simeq 0.8$ is used, rather than the value of $(M/L_I) = 2\pm1$ assumed by Navarro & Steinmetz (1999). But our success in matching the TF relation may also in part be due to an underestimation of $V_{2.2}$ due to resolution and gravitational softening limitations. To test this we compare the results of our MR, Ω_b=0.05 simulations including a UVX field of galaxies S1-S4 with the similar HR ones (note that the gravitational softening lengths used are equivalent to Plummer softening lenghts for the MR (HR) runs of about 1.0 (0.5) and 3.3 (1.6) h^{-1}kpc for the SPH and DM particles respectively, so at least for the HR runs the softening lengths are considerably smaller than $R_{2.2}$ = 5-8 h^{-1} kpc). For the four MR runs we find an average $< \log(V_{2.2}) >_{MR} = 2.367\pm0.017$ and for the four HR runs $< \log(V_{2.2}) >_{HR} = 2.380\pm0.015$. Hence the median $V_{2.2}$ of the HR runs with 8 times the DM mass resolution and half the softening lengths is just $3.1 \pm 5.4\%$ larger than that of the similar MR runs, indicating that resolution and gravitational softening length limitations are not a problem. Our results may therefore indicate that WDM halos are less concentrated than CDM halos. Very high resolution simulations of the formation of WDM halos with and without gas should clearly be undertaken to address this issue properly. Such a program has already been initiated by Moore et al. (1999b): They carried

out a WDM, N-body, very high resolution cluster simulation using a step-function CDM to WDM transfer function, like us, and with $M_{f,WDM}/M_{200} \simeq 0.15$, quite similar to the $M_{f,WDM}/M_{200} \simeq 0.09$-$0.14$ in our WDM2 simulations. They found that the WDM halo was only marginally less concentrated than the corresponding CDM one. Nevertheless, in our view, more very high resolution simulations of this sort should be carried out for galaxy dark matter halos, in particular in low Ω_M cosmologies, to get better statistics. Also, very high resolution simulations including gas should be undertaken to study the effects of central, baryonic "pinching" of the WDM and CDM galaxy halos - these effects could be different if the two sorts of halos have different phase-space distribution functions.

As argued by, e.g., Kravtsov et al. (1998), Moore et al. (1999b) and Navarro & Steinmetz (1999) (but see also van den Bosch et al. 1999) it is quite likely that CDM halos have too much dark matter in their central parts compared to the observed dynamics of dwarf and disk galaxies, thereby resulting in model disk galaxies with too low mass-to-light ratios when compared with the observed (mostly I-band) TF relations. We now estimate a general upper limit to the (M/L_I) of disk galaxies by assuming that disks are "maximal", i.e. as dominant in the inner part of the galaxies as possible given the rotation curve constraints: Maximal disk galaxies have $\gamma \equiv V_{2.2,D}/V_{2.2} \simeq 0.85$ (e.g., Sackett 1997), where $V_{2.2,D}$ is the (peak) rotation velocity of the disk alone at $R_{2.2}$. The disk mass can be expressed as $M_D = f_D M_b$, where M_b is the total, baryonic disk galaxy mass (central component + bulge + disk - neglecting the stellar halo and, for notation, assuming that dark matter is non-baryonic). For an exponential disk

$$V_{2.2,D} = 0.62 \sqrt{\frac{GM_D}{R_D}} \quad . \tag{16}$$

Using this, equation (14) and the definition of γ we then obtain

$$M_b = 4.2 \cdot 10^{10}\ h^{-1}\ \left(\frac{f_D}{0.8}\right)^{-1} \left(\frac{\gamma}{0.85}\right)^{2} \left(\frac{V_c}{200\ \mathrm{km/s}}\right)^{3.05}\ M_\odot \quad . \tag{17}$$

Following Giovanelli et al. (1997) the I-band TF relation can be expressed as

$$L_I = 2.1 \cdot 10^{10}\ h^{-2}\ \left(\frac{V_c}{200\ \mathrm{km/s}}\right)^{3.07}\ L_{I,\odot} \quad , \tag{18}$$

so the I-band mass-to-light ratio of a disk galaxy is given by

$$(M/L_I) = 2.0\ h\ \left(\frac{f_D}{0.8}\right)^{-1} \left(\frac{\gamma}{0.85}\right)^{2} \left(\frac{V_c}{200\ \mathrm{km/s}}\right)^{-0.02}\ M_\odot \quad . \tag{19}$$

Adopting $f_D \gtrsim 0.8$ for Sb-Sd galaxies (e.g., Broeils & Courteau 1997), $\gamma \lesssim 0.85$ (maximal or sub-maximal disks) and neglecting the very weak V_c dependence, we obtain

$$(M/L_I) \lesssim 2.0\ h \tag{20}$$

for intermediate to late type disk galaxies, which for h=0.7 translates into $(M/L_I) \lesssim 1.4$. This is likely to be a generous upper limit as disk galaxies may well be sub-maximal ($\gamma < 0.85$) - see, e.g., Courteau & Rix (1999). The estimated upper limit in equation (20) corresponds very well to the various dynamical and spectrophotometric estimates discussed above, for $h \sim 0.7$.

5.3. The total baryonic mass of the Milky Way as a constraint on disk galaxy formation simulations

Another observational check of the results is obtained by comparing the final disk masses as a function of V_c with the observed, baryonic mass of the Milky Way: Flynn & Fuchs (1994) find a dynamically determined local disk surface density of 52±13 $M_\odot$ /pc^2, out of which about 20-25% is gas. Assuming that the Galactic disk is exponential and that the Sun is situated at R=8 kpc, the total disk mass can be calculated as a function of the exponential scale-length R_D. The result is shown in Figure 18 (solid line) together with the observational 1-σ contours. This provides a lower limit to the baryonic mass of the Milky Way (the radial gas surface density profile is somewhat shallower than that of the stars, but the effect of this on the total disk mass is small, especially since only about 10% of the baryonic mass of the Milky Way is gas).

An upper limit can be obtained by taking into account the mass of the central component (CC)/bulge also. This mass component is highly centrally concentrated, so for our purpose we simply assume that it is located at the center and characterized by a Keplerian rotation curve. We now demand that the combined disk/CC/bulge rotation curve should not exceed the observed value of $\lesssim$ 200 km/s at R=3 kpc (Rholfs et al. 1986) and in this way obtain the CC/bulge mass upper limit shown in Figure 18 (short-dashed line) together with lower and upper 1-σ contours (long-dashed lines) corresponding to the upper and lower ones for the disk mass. The combined disk/CC/bulge upper 1-σ mass limit for the Milky Way is shown as a heavy solid line in the Figure. We conclude that the baryonic mass of the Milky Way is somewhere in the range 3 - 7 $\times$ 10^{10} $M_\odot$ with a likely value of about 5 $\times$ $10^{10} M_\odot$. We adopt a characteristic circular velocity of the Galaxy of V_c = 220 km/s with a 10% uncertainty and plot the result in Figures 16 and 17. Clearly, our results are compatible with the Milky Way baryonic mass constraint for h=0.5 as well as h=0.7, given the uncertainties.

6. Physical candidates for warm dark matter particles.

In this section we discuss possible elementary particle candidates for WDM. There are no established elementary particles with the necessary properties, i.e. stable on cosmological time scales and light, $m_w \sim 1$ keV, to give a free-streaming mass of $\sim 10^{11} M_\odot$ cf. equation (6) (in this section we use the system of units with $c = \hbar = k_B = 1$). Still such particles, which we shall denote *warmons* in the following, are not excluded and may be even natural in some theoretical models:

It is natural to start with massive neutrinos, firstly, because neutrinos, in contrast to other possible dark matter particles are known to exist and, secondly, they may be massive. Direct experiments (Caso et al. 1998) set upper limits of a few eV for the ν_e mass, 160 keV for the ν_μ mass, and 18 MeV for the ν_τ mass. Thus some neutrinos could in principle be warm. However indications of neutrino oscillations found in atmospheric neutrinos demand a very small mass difference between oscillating neutrinos, $\delta m^2 \approx 0.01$ eV^2 (Super-Kamiokande Collaboration 1998). The latter could be $\nu_\mu \leftrightarrow \nu_\tau$ or $\nu_\mu \leftrightarrow \nu_s$, where ν_s is a new sterile neutrino with much weaker interactions than the usual ones. An explanation of the solar neutrino deficit by neutrino oscillations also demands a very small mass difference, now between ν_e and some other active or sterile neutrinos (for a discussion, see, e.g., Bahcall et al. 1998). These results indicate that most neutrino masses are quite small, below or in the eV region. Still neither theory nor experiment excludes that some neutrinos may have masses in the keV range and be warmons.

A usual argument against this hypothesis is that according to the Gerstein-Zeldovich (1966) and Cowsik & MacLelland (1972) limit neutrinos with the *normal weak interactions* give the following contribution to the cosmological mass density:

$$\Omega_\nu h^2 = m_\nu / 94\text{eV} \tag{21}$$

and for such $m_\nu \sim$ keV neutrinos would over-close the universe. A possible way to save neutrinos as warmons is to assume that they have a new interaction stronger than the usual weak one so that their annihilation in the early universe is more efficient and their cosmological number density is one-two orders of magnitude smaller than the standard one, $n_\nu^{(0)} = 110/\text{cm}^3$.

The necessary value of the cross-section of neutrino annihilation can be found from the following considerations. The rate of neutrino annihilation is given by $\dot{n}_\nu / n_\nu = \sigma_{ann} n_\nu$. The annihilation would effectively continue till this rate becomes smaller than the expansion rate $H = \dot{a}/a$. In the cosmological plasma consisting of electromagnetic radiation and three neutrino species with temperature $T_\nu = 0.7 T_\gamma$, the Hubble parameter is $H \approx 3 T_\gamma^2 / m_{Pl}$, where the Planck mass $m_{Pl} = G^{-1/2}$ in our units. If we request that annihilation effectively

ceased when the neutrinos became non-relativistic, $T_\nu < m_\nu$, we obtain as a crude estimate for the relative suppression of the present day neutrino number density with respect to the standard cosmological number density of massless neutrinos the following result:

$$\frac{n_\nu^{(m)}}{n_\nu^{(0)}} \approx \frac{65}{\sigma_{ann} m_{Pl} m_\nu} \tag{22}$$

Subsequent annihilation after freeze-out further increases the suppression by a factor of a few, so we assume as a crude estimate $n_\nu^{(m)}/n_\nu^{(0)} \approx 10/(\sigma_{ann} m_{Pl} m_\nu)$ which is sufficient to get a feeling for the necessary strength of the anomalous $\nu\nu$-interaction. Correspondingly, to contribute a fraction Ω_w of the critical cosmological mass density at present, the cross-section of massive neutrino annihilation should be

$$\sigma_{ann} \approx \frac{10}{94\,\mathrm{eV}\, m_{Pl} \Omega_w h^2} \approx 4 \cdot 10^{-39} \mathrm{cm}^2/(\Omega_w h^2) \quad . \tag{23}$$

The possible annihilation channels are either a pair of massless (or lighter) neutrinos or a pair of light pseudogoldstone bosons, e.g. majorons. We shall return to a possible coupling to majorons below.

"Normal" neutrinos decoupled from the cosmic plasma at $T = 2 - 3$ MeV. However if there is a new and stronger interaction with the annihilation cross-section (23), neutrino self-interaction would remain efficient to much lower temperatures $T \approx m_\nu/4 - m_\nu/5$. Until then the mean-free path of the neutrinos is determined by their annihilation cross-section and would be considerably shorter than the horizon. This could reduce the scale at which perturbations are erased in comparison with more conventional dark matter, which will be free-streaming for $T \gtrsim m_\nu$ (see below). However in this model there exists a new mechanism for dissipation of perturbations at small scales, namely $\nu\nu$-annihilation. The larger the number density of neutrinos the stronger the annihilation (proportional to n_ν^2) and thus neutrinos disappear faster in regions with higher neutrino density, reducing the density contrast. More detailed calculations are necessary to quantitatively understand this effect, but in any case the characteristic scale of damping of fluctuations in this model is roughly equal to the horizon size when $T_\nu \sim m_\nu$ (or somewhat smaller, as argued above), i.e. $t_U \sim 10^6\ (m_\nu/\mathrm{keV})^{-2}$ sec or $z \sim 10^7\ (m_\nu/\mathrm{keV})$.

Before going to the more conventional model of WDM, two comments are worth making. Firstly, in the model discussed above neutrinos are not necessarily the only possible warmons. There could be other convenient particles and in particular light pseudogoldstone bosons. Secondly, with the typical strength of interaction given by eq. (23) warmons would be practically sterile after freeze-out (their mean free path would be $l_f \sim 1/(\sigma n)$ and e.g. for a typical galactic number density $n_{gal} \approx 1/\mathrm{cm}^3$ it would be $l_f \approx 10^{40}$ cm, much larger than the horizon scale). Their self-interaction might be essential if the cross-section for

elastic scattering is much larger than that for annihilation. We would then have a type of dark matter with an essential self-interaction and with a mean-free path possibly much smaller than galactic scales. This could lead to a lowering of the central concentration of dark matter halos - see, e.g., Spergel & Steinhardt (1999). However it is difficult, though in principle possible, to find a natural realization of the model with elastic cross-section much higher than the annihilation one.

Let us now turn to a conventional model of early decoupled particles. This cannot be realized with "normal" neutrinos, so we have a choice of either invoking known particles with new interactions or new particles. They should be light, around a keV, stable and very weakly interacting. They should decouple early when they were relativistic and their number density was equal to the number density of photons, up to a Fermi-Bose factor 3/4 and the number of spin states divided by 2, to normalize to photons. We denote the combination of all these factors g'_w, so that $(n_w/n_\gamma)_{dec} = g'_w$ at the time of warmon decoupling (in this section we use subscript w, rather than the WDM used in the rest of the paper). In the course of expansion and cooling down the number density of photons in the comoving volume increases (entropy dilution) due to annihilation of massive particles in the plasma, so that the relative abundance of warmons decreases. If the cooling proceeded adiabatically, as is most likely, the comoving number of photons increased as g_i/g_f, where $g_{i,f}$ are the numbers of particle species in thermal equilibrium with $m < T$ (with spin and Fermi-Bose factors included, the latter is 7/8 for the entropy density) at initial and final times respectively. When the temperature dropped to ~ 10 MeV there were photons, e^+e^--pairs, and three types of neutrinos in thermal equilibrium (and with $m < T$) with total $g = 10.75$. At smaller temperatures ($T \sim 2 - 3$ Mev) the neutrinos decoupled from the plasma and at $T \sim 1$ MeV e^+e^- annihilation increased the number of photons by 11/4 (see, e.g., Peebles 1993). Thus the present day ratio of the number density of warmons to the number density of photons in the CMB is

$$(n_w/n_\gamma)_0 = 43 g'_w/11 g_{dec} \quad , \tag{24}$$

where g_{dec} is the g defined above (also called the effective number of particle degrees of freedom in section 2) at the time of warmon decoupling.

The contribution of such warmons to the present day "mass density" Ωh^2 would be

$$\Omega_w h^2 = 1.5 \cdot 10^2 \; m_w (g'_w/g_{dec}) \tag{25}$$

where here and below the warmon mass is expressed in keV. This expression is very similar to equation (4) in section 2 for $g'_w \sim 1$. In the minimal standard model the number of particle species above the electroweak scale is $g_{dec} = 107.75$ so the suppression factor is too small to get a small $\Omega_w h^2 \sim 0.1$ with keV mass warmons. In the low energy

supersymmetric extension of the minimal standard model the suppression could be roughly twice stronger, but still not quite enough with keV warmons (unless $\Omega_w \sim 1$). Only for very weak interactions, where decoupling takes place near grand unification scale and if the rank of the unification group is sufficiently high, will the entropy suppression factor be large enough to accommodate warmons with masses of $\sim$ 1 keV and an $\Omega_w h^2 \sim 0.1$.

It is noteworthy that in the case of early decoupled particles their momentum distribution would be considerably softer than that of late decoupled particles, so they would have a smaller free-streaming scale for the same mass. In this model all essential quantities can be expressed in terms of the warmon mass, m_w, and the cosmological "mass density" of warmons, $\Omega_w h^2$ (and g'_w). To calculate the warmon free-streaming length one needs to know the ratio of the warmon temperature when they are relativistic (or average energy if they are not in a thermal state) to the photon temperature. Following the arguments given above this ratio can be expressed as

$$\frac{T_w}{T_\gamma} = \left(\frac{43}{11 g_d}\right)^{1/3} = 0.3 \left(\frac{\Omega_w h^2}{g'_w m_w}\right)^{1/3} \tag{26}$$

We assume that the warmons became non-relativistic and stopped at $T_w = m_w/3$. The physical warmon path in the expanding frame of reference at this time is approximately equal to $l_w = 2t$, where t is the age of the universe, which is related to the photon temperature as $t/\mathrm{sec} \approx 1.7 (T_\gamma/\mathrm{MeV})^{-2}$ for $T_\gamma \lesssim 1$ MeV (we assume that for temperatures below about 1 MeV the universe was dominated by photons and three massless neutrinos with $T_\nu = 0.7 T_\gamma$, until it became matter dominated). It then follows that the warmon free-streaming length is given by

$$l_w = 2.6 \cdot 10^6 \,\mathrm{sec}\, m_w^{-8/3} (\Omega_w h^2 / g'_w)^{2/3} \quad . \tag{27}$$

To calculate the corresponding comoving free-streaming scale $R_{f,w} = (1 + z_w) l_w$ we determine $(1 + z_w)$ as

$$(1 + z_w) = \frac{T_\gamma}{T_\gamma^{(0)}} = \frac{m_w^{4/3}}{0.9 T_\gamma^{(0)}} \left(\frac{g'_w}{\Omega_w h^2}\right)^{1/3} = 4.7 \cdot 10^6 \; m_w^{4/3} \left(\frac{g'_w}{\Omega_w h^2}\right)^{1/3} \quad , \tag{28}$$

where $T_\gamma^{(0)}$=2.4·10^{-7} keV (corresponding to 2.73 K) is the present temperature of the CMB. Hence we obtain after some manipulation

$$R_{f,w} = 0.23 \; (g_{dec}/100)^{-4/3} \; (\Omega_w h^2)^{-1} \; g'_w \;\; \mathrm{Mpc} \quad , \tag{29}$$

very similar to equation (3) in section 2 for $g'_w \sim 1$.

A generic theoretical problem in finding elementary particle warm dark matter candidates is the smallness of their mass on the particle physics scale. On the other hand,

we know that, though do not understand why, most "normal" neutrinos probably are *too* light, so to be warmons, they must have some unusual properties, either to possess stronger than normal weak interactions or vice versa, to be almost sterile. A possible example of the latter are the right-handed neutrinos considered by Malaney et al. (1995) and Colombi et al. (1996).

If neutrinos are not WDM particles, then the next best candidate is probably the majoron (Berezinsky & Valle 1993, Babu et al. 1993, Dolgov et al. 1995). Majorons are light pseudogoldstone bosons (we denote them J in what follows), related to spontaneous breaking of symmetry between lepton families. They could quite naturally have a mass in the keV range and with a reasonable choice of the values of parameters they could give $\Omega_w \sim 0.1$. If one assumes that majorons indeed exist, they could either be warmons themselves or would open such a possibility to neutrinos because the Yukawa coupling $gJ\bar{\nu}\gamma_5\nu$ introduces a new interaction that would permit neutrinos to avoid the Gerstein-Zeldovich limit due to a more efficient annihilation into lighter neutrinos or majorons (here g is the coupling constant and J is the majoron field).

There are several possible options in the majoron scenario. Let us assume first that majorons are warmons and that they are heavier than all neutrinos. In that case the majorons would decay into $\bar{\nu}\nu$-pairs on a time-scale of $\tau_J = (g^2 m_J/4\pi)^{-1}$. Demanding that majorons are stable on the present cosmological time scale, $\tau_J > t_U \approx 10$ Gy, we obtain $g < 10^{-20}/m_J/\mathrm{keV}$. In the simplest version of the model the coupling constant is expressed through the ratio of neutrino mass to the symmetry breaking scale, $g = m_\nu/f$, and the small value of g implies a reasonably high symmetry breaking scale, $f \sim 10^{11}$ GeV for eV-mass neutrinos. In such a model majorons would be warmons, while eV-mass neutrinos could be hot dark matter particles. However very weakly coupled majorons might never have been abundantly produced in the primeval plasma and hence their present day number density would be too low. This would be the case if majorons were coupled only to light neutrinos, but this is not necessarily so and a much stronger coupling to heavy particles is possible and quite natural. It would permit a copious production of majorons at high T, but could come into conflict with the request for their early decoupling. A possible way out of this difficulty is to assume that majorons have never been in thermal equilibrium and were produced in just the amount necessary to be warmons with $\Omega_w h^2 \sim 0.1$. Another and more natural possibility is that majorons only interacted with very heavy particles and when these particles disappeared from the plasma, as T became smaller than their masses, the majorons decoupled at these temperatures.

There is another possible way of cosmological creation of pseudogoldstone bosons, not thermally but through a phase transition. In this case the particles are produced at

rest like, e.g., axions, which are cold dark matter despite being extremely light. Similarly majorons would be also cold and a mechanism to warm them up is required. This could be realized if they have a sufficiently strong self-interaction, λJ^4 (where λ is the coupling constant and J is the majoron field). In the lowest order in this interaction it describes elastic majoron-majoron scattering. In higher orders it gives rise to inelastic processes and in particular describes majoron self-destruction). The majoron annihilation in a model of this kind would be different from the usually considered case. Majorons would predominantly disappear in $4J \to 2J$-reactions. Thus this process not only reduces the number density of majorons but also heats them up. The freezing of species by $4 \to 2$ or $3 \to 2$-reactions and properties of the corresponding dark matter has been considered by Dolgov (1980), Carlson et al. (1992), Machacek et al. (1994), de Laix (1995) and Dolgov et al. (1995). Depending upon the efficiency of the cooling and on the initial majoron momentum distribution this model would supply dark matter somewhat warmer or colder than warm. However majorons in this model would be rather strongly self-interacting, so that their mean free path may be sub-galactic and hence this is another way by which dark matter can be effectively self-interacting.

It is even possible that both thermal and phase transition mechanisms are effective, so that the same particles form both cold and warm dark matter. In this case the coupling of majorons to matter and their self-coupling should be sufficiently weak to avoid a significant mixing between warm and cold majorons. If so, this opens up for the exciting possibility, that compared to CDM one could have smaller, but *non-vanishing* power on mass scales less than the WDM free-streaming scale ($\sim 10^{10}$-$10^{11} M_\odot$).

Another possible case of interest is that some of the neutrino species are heavier than majorons. In that case the heavier neutrinos would decay into majorons and lighter neutrinos. This was considered in several papers dealing with unstable dark matter - see, e.g., Dolgov (1999) and references therein. We are not interested here in the shift of the epoch of equivalence between matter and radiation due to decay of massive non-relativistic particles into relativistic products, so we do not request that the life-time of the heavy neutrinos should lie in a specific interval around a year plus-minus a few orders of magnitude. It could be much shorter as well as much longer. If the neutrino life-time is sufficiently short they would not contribute to the cosmic dark matter and we remain with majorons. However, the non-diagonal coupling of majorons to neutrinos may be very small so that heavier neutrinos would be quite stable (see below) and hence be the dark matter, while majorons could be unimportant in this respect. There are two possible annihilation channels of heavy neutrinos, into two light ones, $\nu_h \nu_h \to \nu_l \nu_l$ or into two majorons. Since the coupling of majorons to neutrinos is generically proportional to the neutrino mass, the first process would be subdominant, if only heavy neutrinos and majorons are not nearly

mass degenerate. In the simplest model the cross-section of the process $\nu_h\nu_h \to 2J$ can be estimated as

$$V\sigma_{2\nu_h\to 2J} \sim g^4/m^2_{\nu_h} \tag{30}$$

where V is the c.m. velocity of annihilating particles. This process could reduce the cosmological abundance of the heavy neutrinos to avoid conflict with the Gerstein-Zeldovich limit. To have a neutrino mass in the keV range requires $g^4 \sim 10^{-23} m_w^2/\Omega_w h^2$ (here $m_w \equiv m_{\nu_h}$).

One should keep in mind that light majorons would be abundantly produced in stars and might strongly influence stellar evolution. This gives rise to a quite strong restriction of the majoron parameter space (for a discussion see, e.g., Raffelt 1996). In particular, to avoid an excessive cooling of supernovae through majoron emission, the mean free path of majorons inside the star should be smaller than its radius. For a supernova with $T = 10$ MeV it is $l_{free} = 1/\sigma n_\nu \approx 10^{10}\,\mathrm{cm}(10^{-5}/g)^4$. So one needs a rather strong coupling, $g > 10^{-5}$. This may be in a potential conflict with the estimate given above.

A very interesting, though seemingly unnatural, possibility is that majorons and heavy neutrinos have masses in keV range, so that both contribute to warm dark matter. However for such a two-component WDM model the problem of cosmic conspiracy, i.e. of near equality of the contributions of different forms of dark matter to Ω, becomes especially frustrating.

Another possibility is to keep neutrinos rather heavy (in the MeV range), unstable and relatively short-lived, while keV majorons, produced by neutrino decays when the number density of neutrinos was already Boltzmann suppressed, would be dark matter particles. Special care should be taken, however, that the majorons produced in this way would be cool enough to be warmons, as they might be more energetic than normal thermal equilibrium ones. Such cooling may be achieved by either elastic scattering of majorons on the remaining heavy neutrinos if the diagonal coupling responsible for elastic scattering is much larger than the non-diagonal one responsible for the decay or by elastic scattering of majorons on themselves. To avoid a conflict with big bang nucleosynthesis (see, e.g., Dolgov et al. 1997), the heavy neutrinos should have an additional anomalous interaction suppressing their number density at BBN.

A new zoo of interesting candidates for dark matter particles is opened up if mirror or shadow worlds exist. These are whole new worlds of new elementary particles that are similar or exactly the same as ours and are coupled to our world only through gravity and/or possibly through a new and very weak interaction. A list of references and a discussion of the subject can be found, e.g., in Dolgov (1999). Shadow world neutrinos, as

considered by Berezhiani & Mohapatra (1995) and Berezhiani et al. (1996) could look in our world as sterile ones and have a mass in the keV range. Their number density would be sufficiently suppressed if the temperature of the shadow world is smaller than ours and they would be excellent warm dark matter candidates. Finally, new dark matter particles, including some which may be WDM candidates, have been recently considered by Garriga & Tanaka (1999), Arkani-Hamed et al. (1999) and Csáki et al. (1999) in the framework of multidimentional cosmologies. Phenomenologically they are rather similar to shadow particles.

In summary, there are plenty of particle physics candidates for warmons. Their properties and initial momentum distributions may be significantly different. They could be self-interacting or sterile, long-lived or absolutely stable. To mention a few, they could be neutrinos with weaker or stronger couplings than normal, majorons (light pseudogoldstone bosons) or shadow or mirror world neutrinos.

7. Discussion and conclusions

In conclusion we find it quite likely that the disk galaxy angular momentum problem can be *completely* resolved by going to the WDM cosmological structure formation scenario without having to resort to star-burst driven feedback processes at all. For Ω_M=1 our results suggest that this requires the WDM free-streaming mass to be $M_{f,WDM} \sim 10^{11} h^{-1} M_\odot$ within about a factor of three, indicating that extreme fine-tuning is not required. This range of characteristic free-streaming masses corresponds to characteristic wavenumbers $k_c \sim$ 5-10 h Mpc^{-1}. For wavenumbers about 2-3 times larger than this the WDM power spectrum is significantly reduced relative to the CDM one, cf. Figure 1. In the interesting work by Croft et al. (1999) the linear power spectrum is determined "observationally" from the Lyα forest in spectra of quasars at <z>=2.5 for wavenumbers in the range 0.3-0.5$\lesssim k \lesssim$ 2-3 h Mpc^{-1}. In this range of wavenumbers the measured $P(k)$ is found to compare well with CDM power spectra. If this method can be pushed to about 4 times larger wavenumbers, it would be possible to test directly the hypothesis that dark matter is warm, with the characteristics proposed in this work, rather than cold. In fact, McDonald et al. (1999) have been able to push the method to about twice as large wavenumbers by using high dispersion spectra of quasars at somewhat larger redshifts (see also Nusser & Haehnelt 1999), but this is probably as far as one can get using the Lyα forest method (R. Croft, private communication).

Currently there are many indications that Ω_M probably is less than unity, $\Omega_M \simeq 0.3$, say. For such OWDM as well as ΛWDM models the cluster normalized value of σ_8 will be

$\simeq 1$, rather than 0.5 for the Ω_M=1 considered in this paper. Also, the late linear growth is slower in the low Ω models. Taking this together implies that the density fluctuations are about 1.5-2 times larger at redshifts $z \gtrsim \Omega_M^{-1} - 1$ and consequently that galaxy formation is somewhat faster and more intense in low Ω_M models. For such cosmologies it therefore seems reasonable to assume that the WDM free-streaming mass-scales, which will allow large, high specific angular momentum disks to form, will be no less than the ones found in this work for Ω_M=1. From this constraint and equation (6) it follows that the mass of the warm dark matter particle(s) has to be of the order 1 keV with a fairly weak dependence on Ω_{WDM}.

We find a slope of our "theoretical" Tully-Fisher relation which matches that of the observed I-band TF relation very well. In terms of the normalization of the TF relation we find agreement provided that the mass-to-light ratio of disk galaxies is $(M/L_I) \simeq 0.8$ for h=0.7. We argue that this is in reasonable agreement with various recent estimates of (M/L_I), including one given in section 5.2 of this paper. The discrepancy of a factor of ~ 5 in absolute luminosity found by Steinmetz & Navarro (1999) and Navarro & Steinmetz (1999) in matching the observed TF relation, using similar kinds of CDM disk galaxy formation simulations, is at least partly caused by the adoption of a larger mass-to-light ratio ($(M/L_I) \sim 2$) by these authors. But it may also partly be due to a difference between the central structure of WDM and CDM halos, in the sense of the WDM ones being less centrally concentrated. In the light of the failure of CDM halos to account for the observed central dark matter profiles in dwarf and disk galaxies, very high resolution simulations with and without gas should be performed to check this exciting possibility properly. Of particular interest would be low Ω_M WDM simulations, rather than the Ω_M=1 ones presented in this work, since one might expect lower concentration halos to form in such cosmologies, as is the case for CDM.

A potential problem for the WDM scenario might be a lack of a sufficient rate of early galaxy formation to match observations: Lyman break galaxies are routinely found at redshifts 3-4 and galaxies have been detected at even higher redshifts, with a current record of z=6.7 (Chen, Lanzetta & Pascarelle 1999). Assuming that galaxies form from n-σ peaks, where $n \sim$ 2-3 (e.g., Ryden & Gunn 1987), and using linear theory it follows that the typical formation redshift of galaxies of mass M will be $z_f \simeq n\sigma(M; z = 0)/\delta_c - 1$, where δ_c=1.69 (see White 1993). From Figure 2 it follows that for the characteristic WDM free-streaming masses relevant for this work, smaller galaxies ($M \lesssim 10^9$-$10^{10} M_\odot$) will form from 2-σ peaks at typical redshifts $z_f \sim$ 4-5 and from (rarer) 3-σ peaks at $z_f \sim$ 6-8 and larger galaxies somewhat later (but not later than in CDM models as $\sigma(M)$ is almost the same in the WDM1, WDM2 and CDM models for $M \gtrsim 10^{11}\ M_\odot$). For low Ω_M cosmologies the formation redshifts would be expected to be even higher than this, so qualitatively

the WDM scenario does not seem to be in trouble on this point. Moreover, Schaeffer & Silk (1988) found that warm dark matter can provide a galaxy distribution that is close to observed galaxy counts, provided $\Gamma \equiv \Omega_M h > 0.1$, which is likely to be the case. In particular they found that in the warm dark matter structure formation scenario small-scale objects ($M \lesssim 10^{10}\ M_\odot$) are not overproduced, contrary to what may be the case for CDM, cf. section 1.

A general problem for Ω_M=1 models is major (mass ratios $\sim$ 1:4 or more), late merging events, which potentially can be fatal for the fragile, stellar disks. Such late merging events also occur in our WDM simulations of galaxies S2-S4 at redshifts z=0.2-0.4. This provides yet another reason for going to low Ω_M models, since such merging would be expected to take place faster and earlier, leaving more time afterwards for the disks to grow smoothly and steadily from cooling flows and to form stars out of the cool gas.

Finally, from a particle physics point of view, there are plenty of candidates for warmons. Their properties and initial momentum distributions may be significantly different. They could be self-interacting or sterile, long-lived or absolutely stable. It is even possible that the *same* particles form both cold and warm dark matter. If so, the exciting possibility exists, that compared to CDM one could have smaller, but non-zero power on mass scales less than the WDM free-streaming scale ($\sim 10^{10}$-$10^{11} M_\odot$).
To mention a few WDM particle candidates in summary, they could be neutrinos with weaker or stronger couplings than normal, majorons (light pseudogoldstone bosons) or shadow or mirror world neutrinos.

In closing, given the success of WDM scenario in solving the angular momentum problem and possibly other problems related to galaxy formation and structure, N-body and more hydro/gravity simulations should be undertaken in various cosmologies to bring the WDM scenario on a more rigorous footing.

We have benefited from discussions with Per Rex Christensen, Rupert Croft, Fabio Governato, Martin Götz, Ben Moore, Bernard Pagel, Örnólfur Rögnvaldsson, Jens Schmalzing and Joe Silk. This work was supported by Danmarks Grundforskningsfond through its support for the establishment of the Theoretical Astrophysics Center. AD thanks the Issac Newton Institue for Mathematical Science for its hospitality during the completion of this work.

REFERENCES

Arkani-Hamed, N., Dimopoulos, S., Dvali, G., & Kaloper, N. 1999, hep-th/9911386

Babu, K. S., Rothstein. I. Z., & and Seckel, D. 1993, Nucl. Phys. B403, 725

Bahcall, J. N., Krastev, P. I., & Smirnov, A. Yu. 1998, Phys.Rev. D58, 096016

Bardeen, J., et al. 1986, ApJ, 304, 15

Barnes, J., & Efstathiou, G. 1987, ApJ, 319, 575

Berezhiani, Z. G. & Mohapatra, R. N. 1995, Phys. Rev. D52, 6607

Berezhiani, Z. G., Dolgov, A. D., & Mohapatra, R. N. 1996, Phys. Lett. B375, 26

Berezinsky, V., & Valle, J. W. F. 1993, Phys. Lett. B318, 360

Boissier, S., & Prantzos, N. 1999, MNRAS, in press (astro-ph/9909120)

van den Bosch, F. C., et al. 1999, AJ, submitted (astro-ph/9911372)

Broeils, A. H., & Courteau, S. 1997, in Dark and Visible Matter in Galaxies and Cosmological Implications, ed. M. Persic and P. Salucci (ASP, San Francisco), p. 74

Burkert, A. 1995, ApJ, 488, L55

de Blok, W. J. G., & McGaugh, S. S. 1997, MNRAS, 290, 533

Carlson, E. D., Machacek, M. E., & Hall, L. J. 1992, ApJ, 398, 43

Caso, C., et al. 1998, European Phys. J., C3, 1

Chen, H. W., Lanzetta, K. M., & Pascarelle, S. 1999, Nature, 398, 586

Colombi, S., Dodelson, S., & Widrow, L. M. 1996, Ap. J. 458, 1

Courteau, S. 1997, AJ, 114, 2402

Courteau, S., & Rix, H. W. 1999, ApJ, 513, 561

Cowsik, R., & MacLelland, J. 1972, Phys. Rev. Lett. 29, 669

Croft, R. A. C., et al. 1999, ApJ, 520, 1

Csáki, C., Graesser, M., Randall, L., & Terning, J. 1999, hep-th/9911406

Dekel, A., & Silk, J. 1986, ApJ, 303, 39

Dolgov, A. D. 1980, Yadernaya Fizika (Sov. J. Nucl. Phys.), 31, 1522

Dolgov, A. D. 1999, hep-ph/9910532, Invited talk at Gamow's International Conference, St. Petersburg, August, 1999 (to be published in the Proceedings).

Dolgov, A. D., Pastor, S., & Valle, J. W. F. 1995, FTUV/95-14, IFIV/95-14, (astro-ph/9506011)

Dolgov, A. D., Pastor, S., Romao, J. C., & and Valle, J. W. F Nucl.Phys. 1997, B 496, 24-40

Dubinski, J., & Carlberg, R. 1991, ApJ, 378, 496

Efstathiou, G. 1992, MNRAS, 256, P43

Eke, V. R., Cole, S., & Frenk, C. S. 1996, MNRAS, 282, 263

Eke, V. R., Efstathiou, G., & Wright, L. 1999, MNRAS, submitted (astro-ph/9908294)

Flynn, C., & Fuchs, B. 1994, MNRAS, 270, 471

Fall, S. M., & Efstathiou, G. 1980, MNRAS, 193, 189

Fukugita, M., Hogan, C. J., & Peebles, P. J. E. 1998, ApJ, 503, 518

Fukushige, T., & Makino, J. 1997, ApJ, 477, L9

Garriga, G. & Tanaka, T. 1999, hep-th/9911055

Gelato, S., & Sommer-Larsen, J. 1999, MNRAS, 303, 321

Gerstein, S.S. & Zeldovich, Ya. B. 1966, ZhETF Pis'ma Red. 4, 174

Giovanelli, R., et al. 1999, ApJ, 477, L1

Haardt, F., & Madau, P. 1996, ApJ, 461, 20

Heavens, A., & Peacock, J. 1988, MNRAS, 232, 339

Hernquist, L., & Katz, N. 1989, ApJS, 70, 419

Huss, A., Jain, B., & Steinmetz, M. 1999, ApJ, 517, 64

Klypin, A., Kravtsov, A. V., Valenzuela, O., & Prada, F. 1999, ApJ, 523, 32

Kravtsov, A. V., Klypin, A. A., Bullock, J. S., & Primack, J. R. 1998, ApJ, 502, 48

van der Kruit, P. C., & Searle, L. 1982, A&A, 110, 61

de Laix, A. A., Scherrer, R. J., & Schaffer, R. K. 1995, ApJ, 452, 495

Mac Low, M.-M. & Ferrara, A. 1999, ApJ, 513, 142

Madau, P., et al. 1996, MNRAS, 283, 1388

Machacek, M. E. 1994, ApJ431, 41

Malaney, R., Starkman, G., & Widrow, L. M. 1995, Phys.Rev. D52, 5480

McDonald, P., et al. 1999, ApJ, submitted (astro-ph/9911196)

Mo, H. J., Mao, S., & White, S. D. M. 1998, MNRAS, 295, 319

Monaghan, J. J., & Gingold, R. A. 1983, J. Comput. Phys., 52, 374

Moore, B., Governato, F., Quinn, T., Stadel, J., & Lake, G. 1998, ApJ, 499, L5

Moore, B., Ghinga, S., Governato, F., Lake, G., Quinn, T., Stadel, J., & Tozzi, P. 1999a, ApJ, 524, L19

Moore, B., Quinn, T., Governato, F., Stadel, J., & Lake, G. 1999b, MNRAS, submitted (astro-ph/9903164)

Navarro, J. F., & Benz, W. 1991, ApJ, 380, 320

Navarro, J. F., & White, S. D. M. 1994, MNRAS, 267, 401

Navarro, J. F., Frenk, C. S., & White, S. D. M. 1995, MNRAS, 275, 56

Navarro, J. F., Frenk, C. S., & White, S. D. M. 1996, MNRAS, 462, 563

Navarro, J. F., & Steinmetz, M. 1997, ApJ, 478, 13

Navarro, J. F., & Steinmetz, M. 1999, ApJ, in press (astro-ph/9908114)

Nusser, A., & Haehnelt, M. 1999, MNRAS, submitted (astro-ph/9906406)

Peebles, P. J. E. 1980, The Large-Scale Structure of the Universe (Princeton: Princeton Univ. Press)

Peebles, P. J. E. 1993, Principles of Physical Cosmology (Princeton: Princeton Univ. Press)

Persic, M., & Salucci, P. 1992, MNRAS, 258, 14p

Raffelt, G. 1996, Stars as Laboratories for Fundamental Physics (Chicago:University of Chicago Press)

Rohlfs, K., et al. 1986, A&A, 158, 181

Ryden, B. S., & Gunn, J. E. 1987, ApJ, 318, 15

Sackett, P. D. 1997, ApJ, 483, 103

Schaeffer, R., & Silk, J. 1988, ApJ, 332, 1

Sommer-Larsen, J. 1991, MNRAS, 250, 356

Sommer-Larsen, J., Gelato, S., & Vedel. H. 1999, ApJ, 519, 501 (SLGV99)

Spergel, D. N. & Steinhardt, P. J. 1999, astro-ph/9909386.

Steinmetz, M., & Navarro, J. F. 1999, ApJ, 513, 555

Steidel, C. C., et al. 1999, ApJ, 519, 1

Super-Kamiokande Collaboration 1998, Phys. Rev. Lett. 81, 1562

Syer, D., Mao, S., & Mo., H. J. 1997, MNRAS, submitted (astro-ph/9711160)

Thakar, A. R., & Ryden, B. S. 1998, ApJ, 506, 93

Vedel, H., Hellsten, U., & Sommer-Larsen, J. 1994, MNRAS, 271, 743

Weil, M. L., Eke, V. R., & Efstathiou, G. 1998, MNRAS, 300, 773

White, S. D. M., & Rees, M. J. 1978, MNRAS, 183, 341

White, S. D. M. 1993, in Les Houches Session LX, Cosmology and Large Scale Structure, ed. R. Schaeffer et al. (Amsterdam: Elsevier)

Yoshii, Y., & Arimoto, N. 1987, A&A, 188, 13

Zel'dovich, Ya. B. 1970, A&A, 5, 84

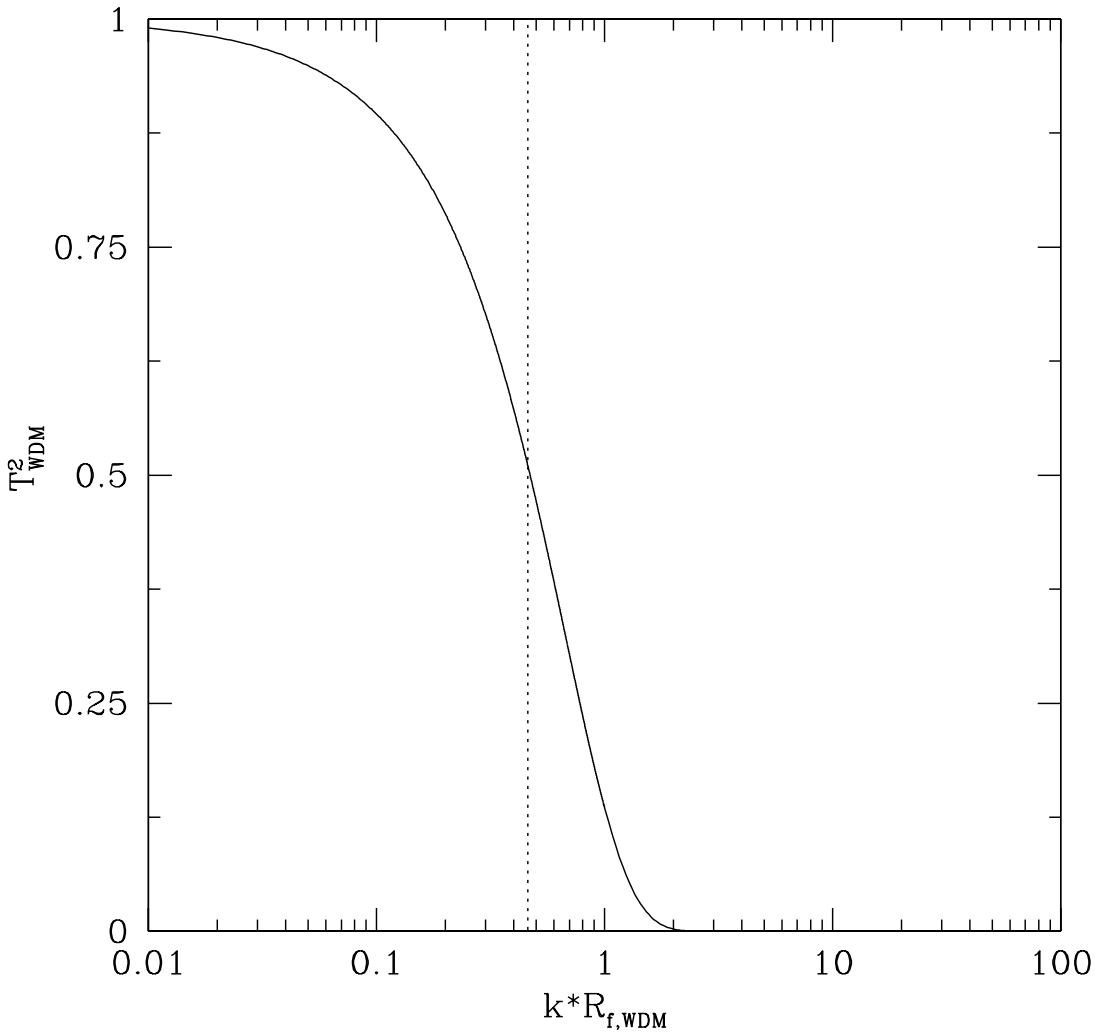

Fig. 1.— The square of the CDM to WDM transfer function (*solid line*) and the step-function approximation used in this work (*dotted line*).

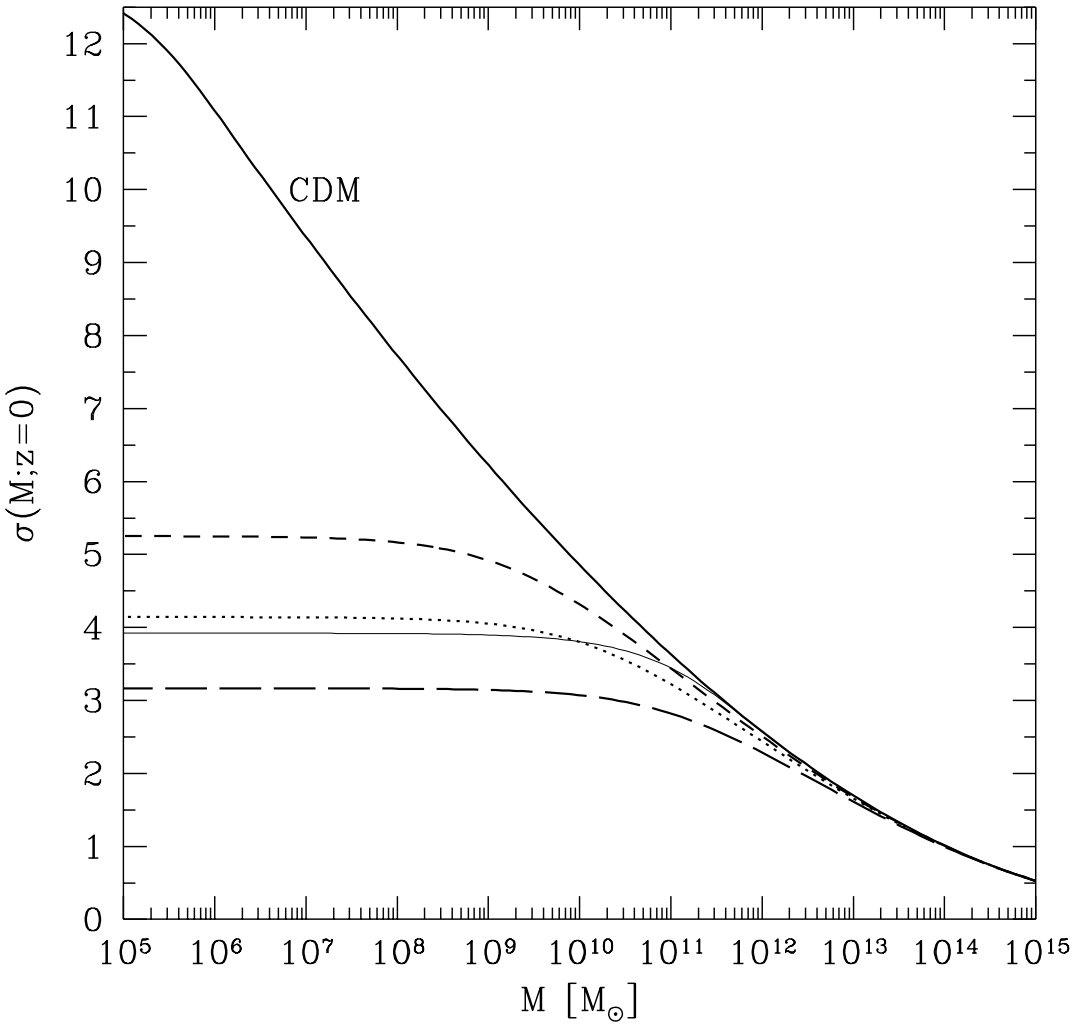

Fig. 2.— The mass fluctuation dispersion $\sigma(M)$ at z=0 for CDM (*heavy solid line*) and three types of WDM with $M_{f,WDM} = 1.9 \times 10^{10} h^{-1} M_\odot$ (*short-dashed line*), $1.5 \times 10^{11} h^{-1} M_\odot$ (*dotted line*) and $1.2 \times 10^{12} h^{-1} M_\odot$ (*long-dashed line*). Also shown is $\tilde{\sigma}(M; z{=}0)$ for our step-function approximation to T_{WDM} for $M_{f,WDM} = 1.5 \times 10^{11} h^{-1} M_\odot$ (*thin solid line*).

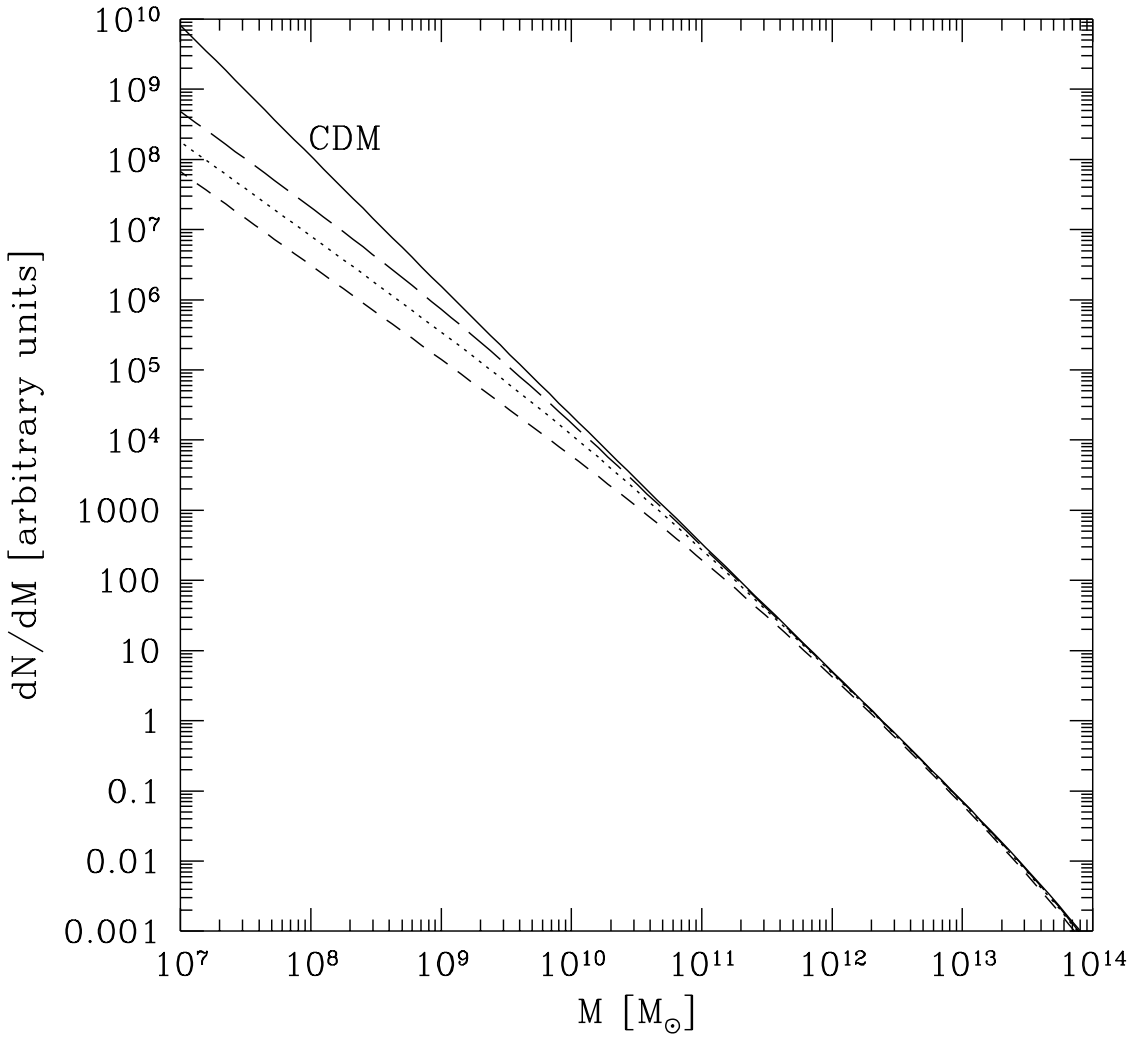

Fig. 3.— Mass spectra, dN/dM, for CDM and the three types of WDM from Fig. 2 (symbols as in Fig. 2).

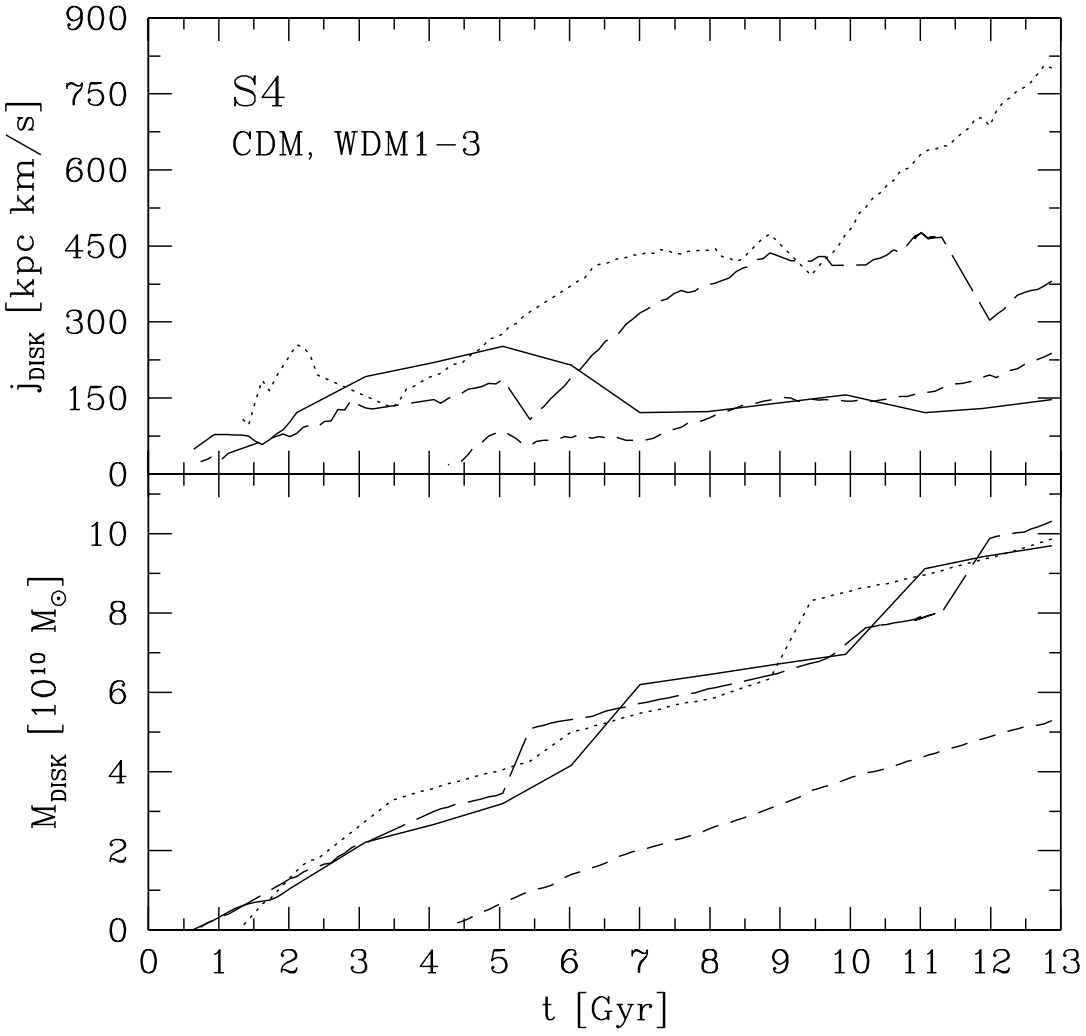

Fig. 4.— Specific angular momenta $j_{disk}(t)$ and cooled-out mass $M_{disk}(t)$ of the disk galaxies forming in the CDM and the three types of WDM simulations (with $\Omega_b = 0.05$ and UVX radiation field) of galaxy S4 - symbols as in Fig. 2.

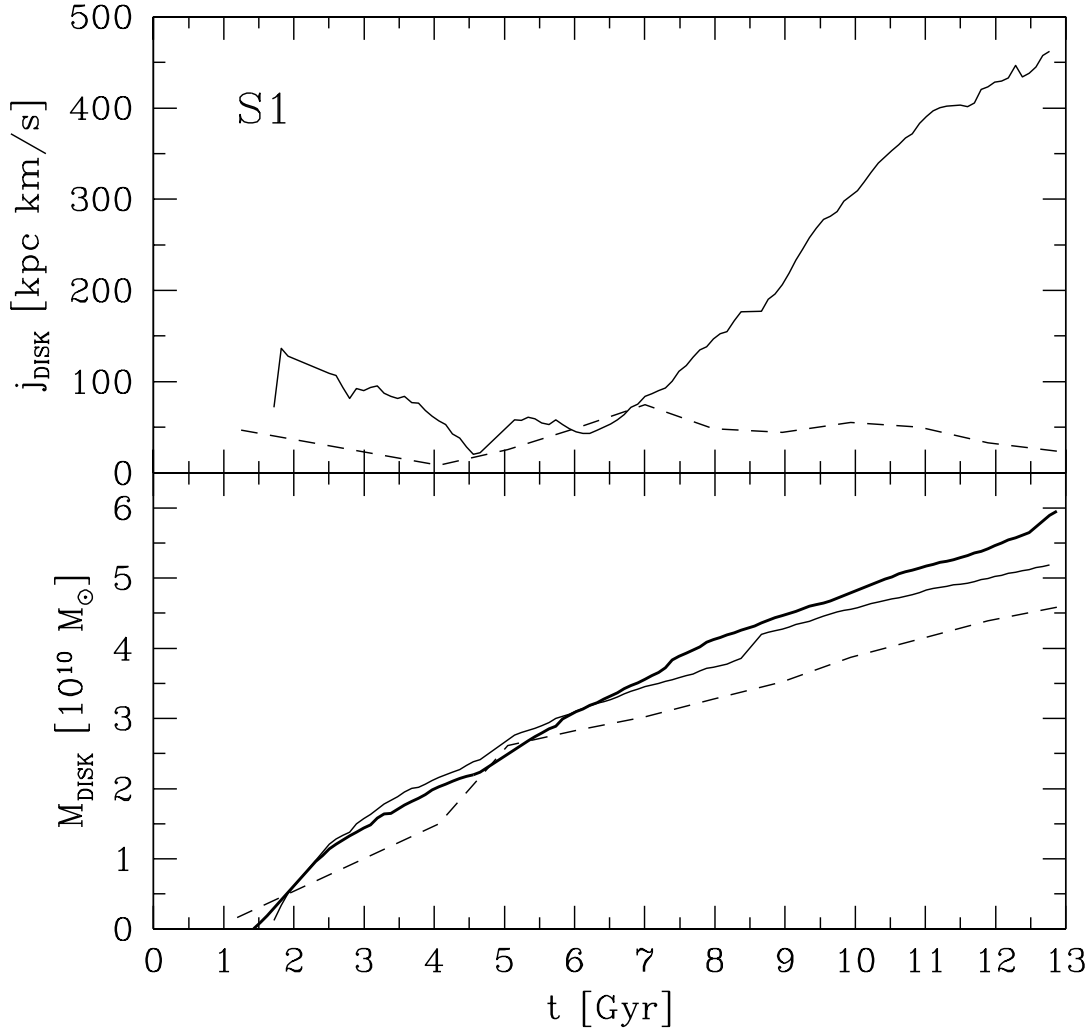

Fig. 5.— Specific angular momenta $j_{disk}(t)$ and cooled-out mass $M_{disk}(t)$ of the disk galaxies forming in the CDM (*dashed lines*) and WDM2, MR (*solid lines*) and HR (*heavy solid lines*) simulations (with $\Omega_b = 0.05$ and UVX radiation field) of galaxy S1 ($j_{disk}(t)$ is not shown for the HR simulation of this galaxy - see text).

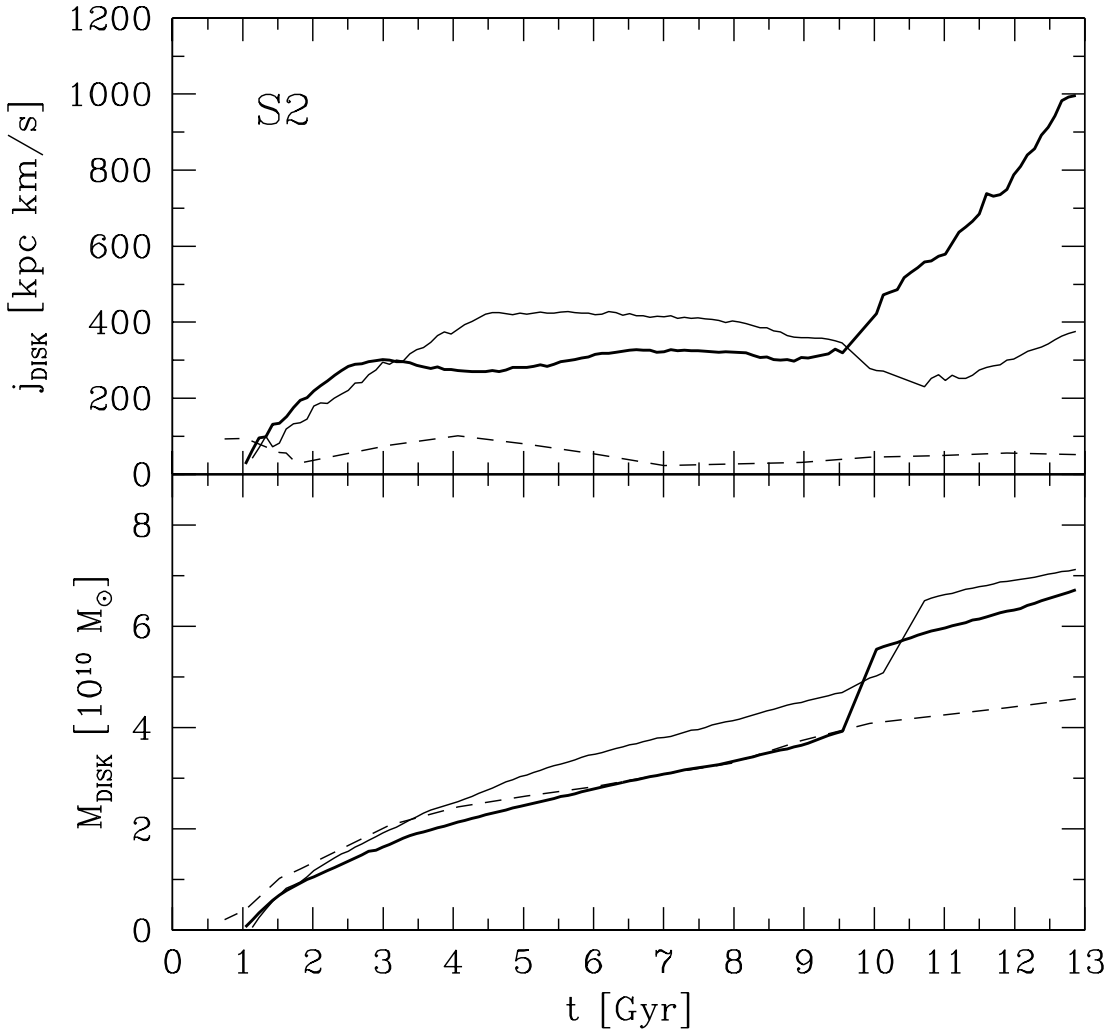

Fig. 6.— Same as in Fig. 5, but for galaxy S2.

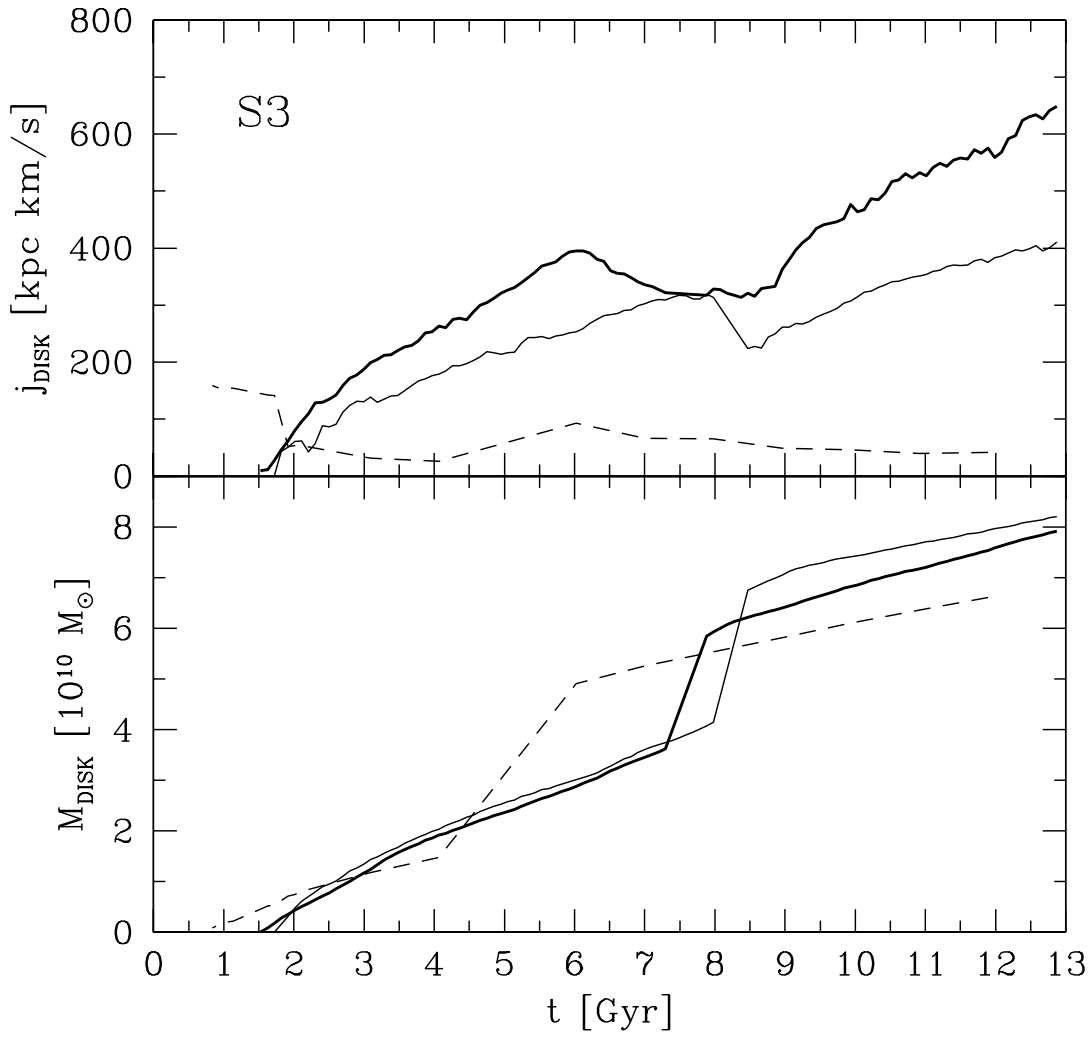

Fig. 7.— Same as in Fig. 5, but for galaxy S3.

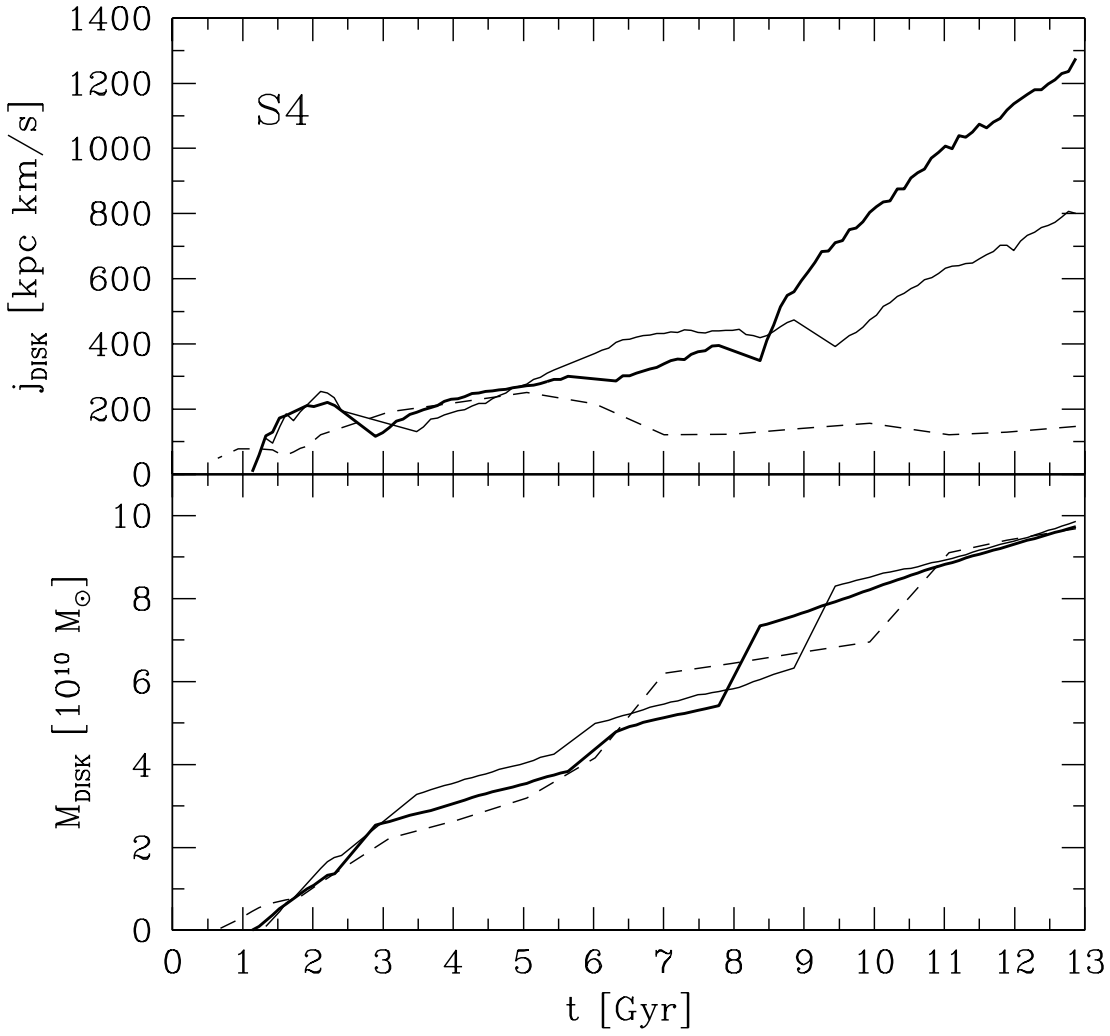

Fig. 8.— Same as in Fig. 5, but for galaxy S4.

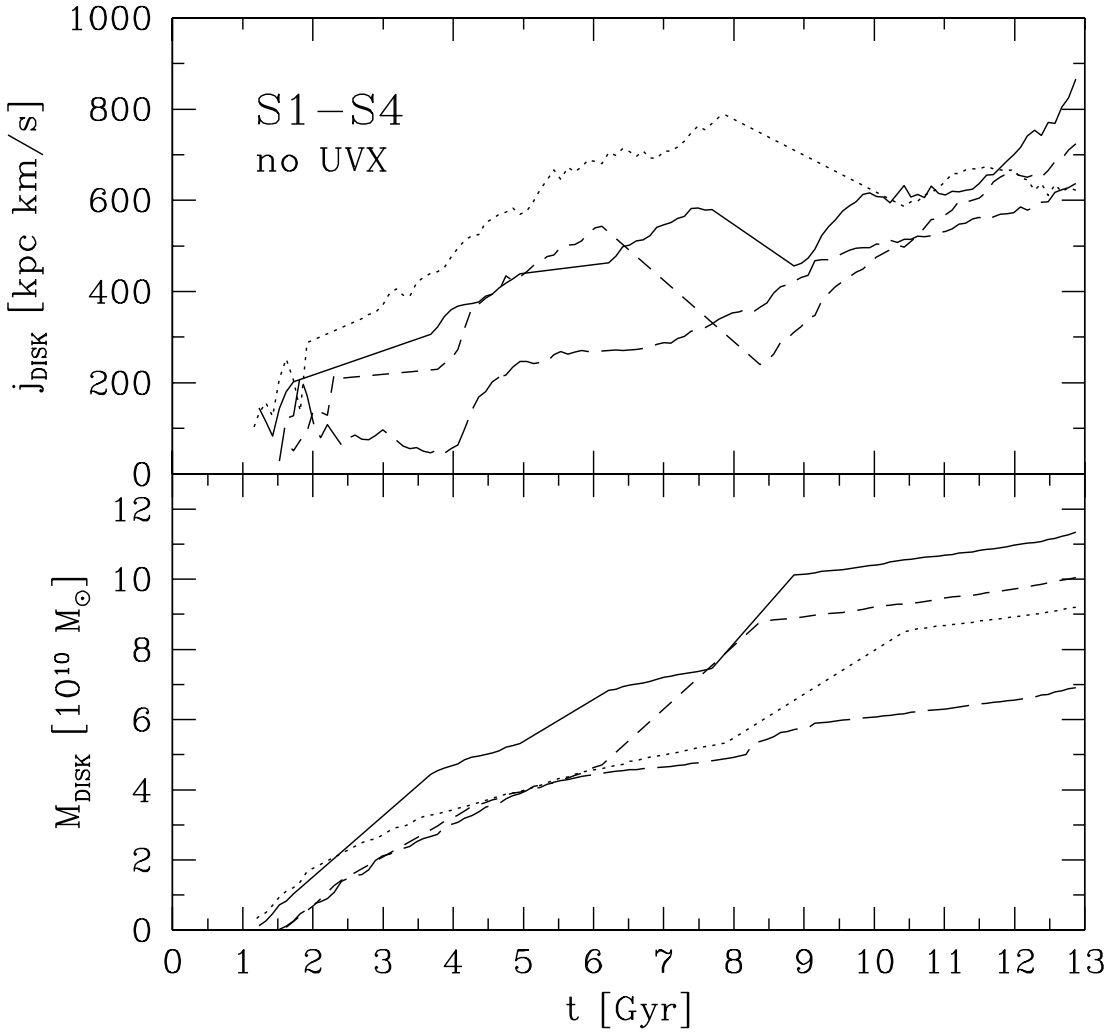

Fig. 9.— Specific angular momenta $j_{disk}(t)$ and cooled-out mass $M_{disk}(t)$ of the disk galaxies forming in the WDM2, MR simulations (with $\Omega_b = 0.05$ and no UVX radiation field) of galaxies S1 (*long-dashed line*), S2 (*dotted line*), S3 (*short-dashed line*) and S4 (*solid line*).

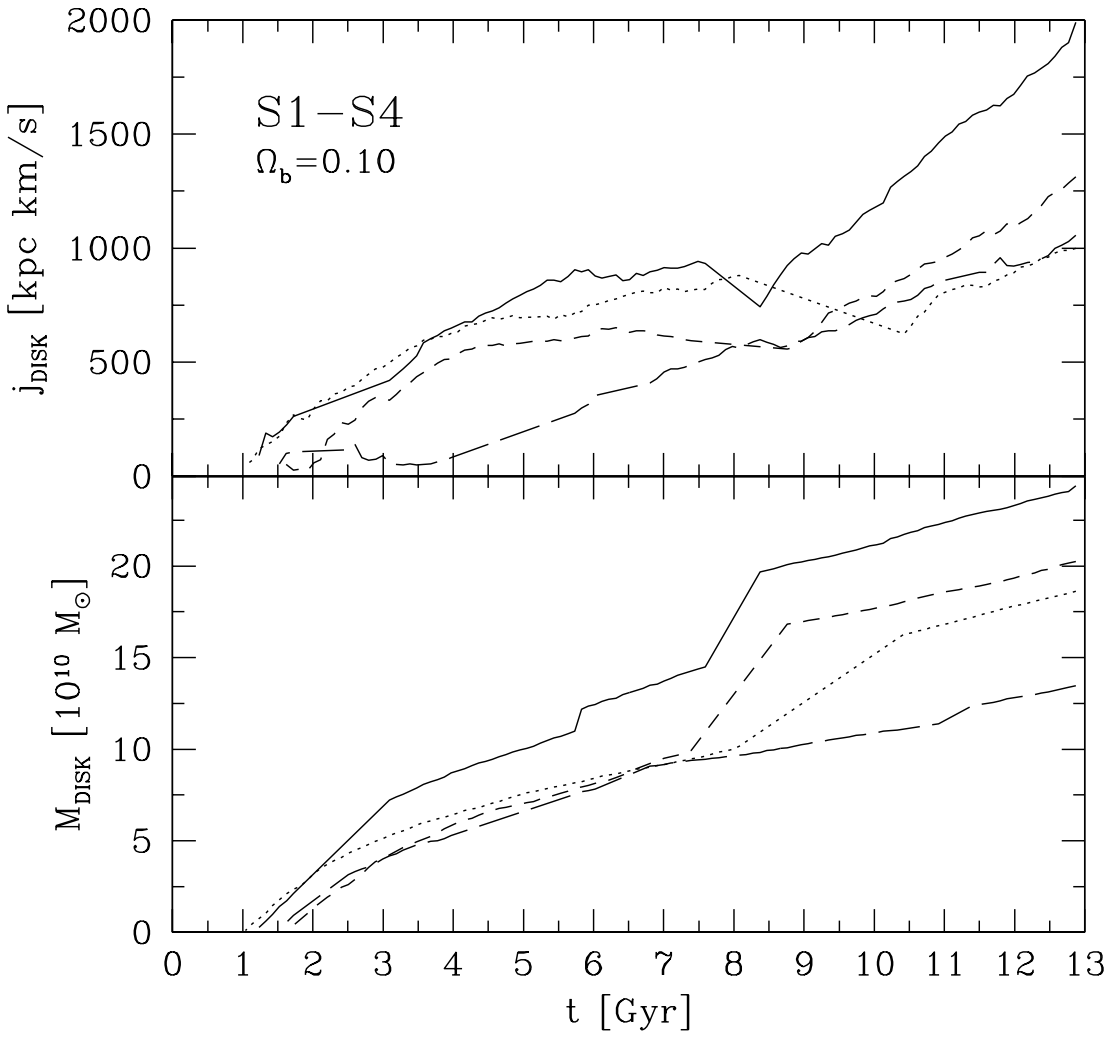

Fig. 10.— Same as in Fig. 9, but with $\Omega_b = 0.10$ and UVX radiation field.

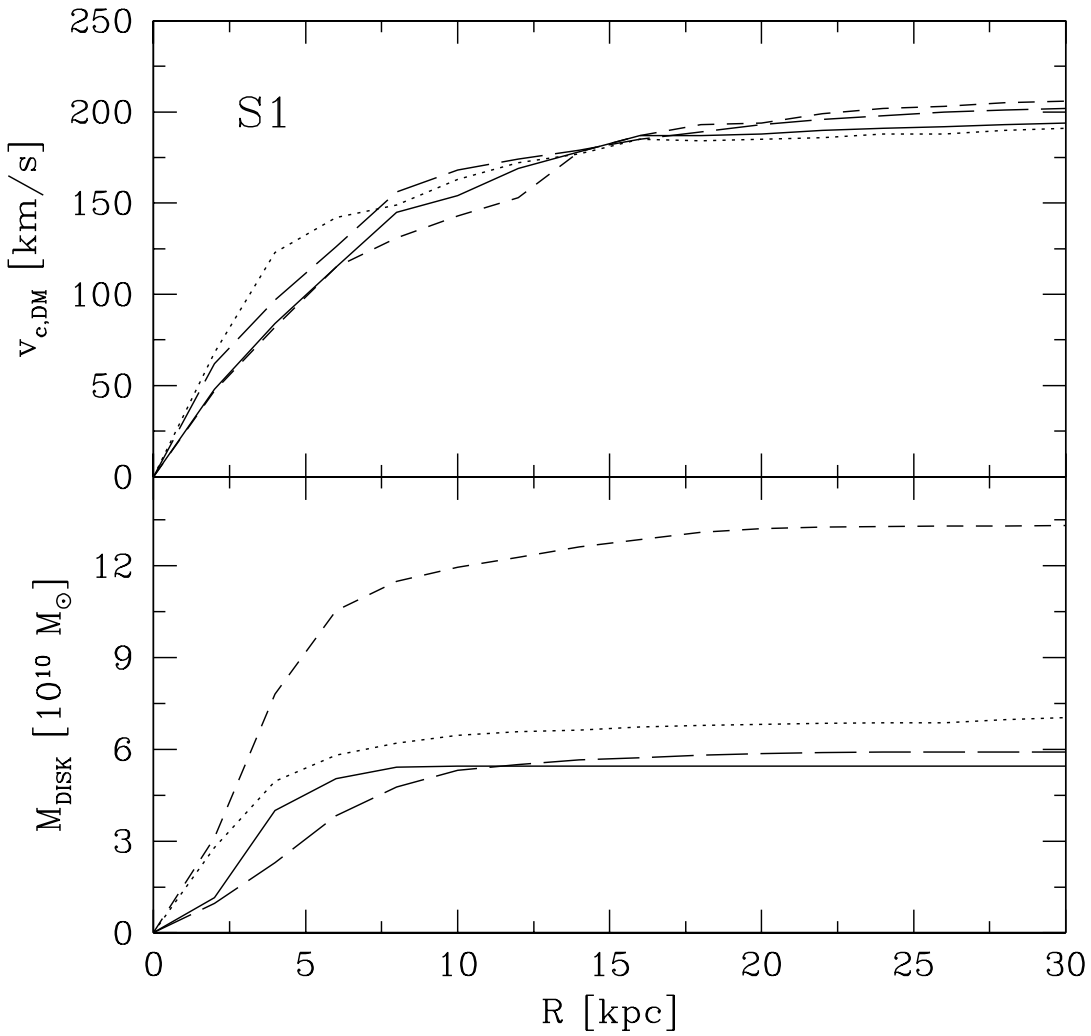

Fig. 11.— Circular velocity $v_{c,DM}(R)$ of the final dark matter halos and cooled-out disk mass $M_{disk}(R)$ of the final disk galaxies formed in the WDM2 simulations of galaxy S1: The MR run with $\Omega_b = 0.05$ and UVX radiation field (*solid lines*), the similar HR run (*long-dashed lines*), the MR run with $\Omega_b = 0.05$ and no UVX radiation field (*dotted line*) and the MR run with $\Omega_b = 0.10$ and UVX radiation field (*short-dashed lines*).

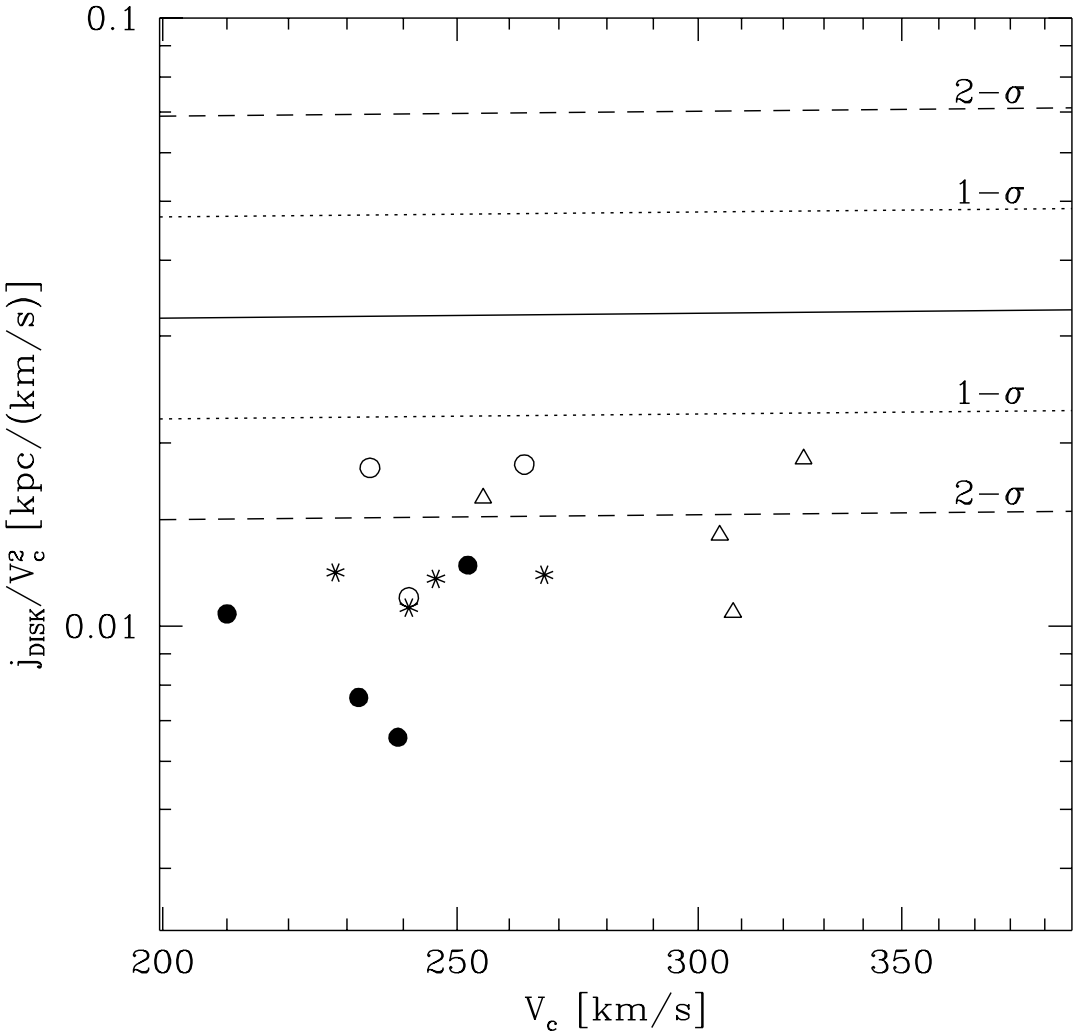

Fig. 12.— Normalized specific angular momenta $\tilde{j}_{\rm disk} \equiv j_{\rm disk}/V_c^2$ of the final disk galaxies formed in the WDM2 simulations: The MR runs with $\Omega_b = 0.05$ and UVX radiation field (*filled circles*), the similar HR run (*open circles*; S1 not shown - see text), the MR runs with $\Omega_b = 0.05$ and no UVX radiation field (*asterisks*) and the MR runs with $\Omega_b = 0.10$ and UVX radiation field (*open triangles*). The solid line shows the median value from the observational data, the dotted and dashed lines bracket the 1-σ and 2-σ intervals around this mean.

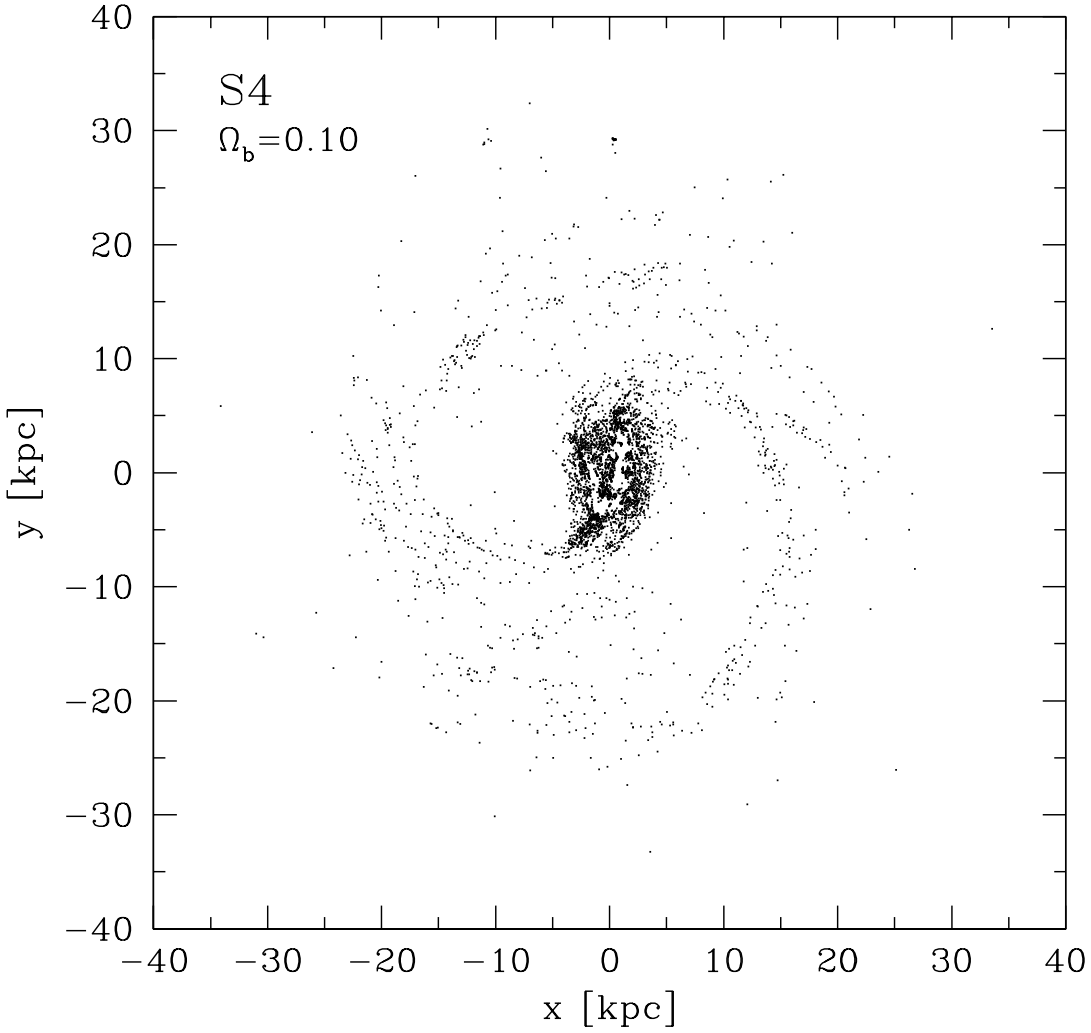

Fig. 13.— Face-on view of the final galaxy formed in run # 18 - this disk galaxy has the largest specific angular momentum of all galaxies formed in our WDM simulations, $j_{disk} \simeq$ 2000 kpc km/s. Shown in the Figure are all $\sim$ 4200 SPH particles in the central disk with $\log(T) < 4.5$.

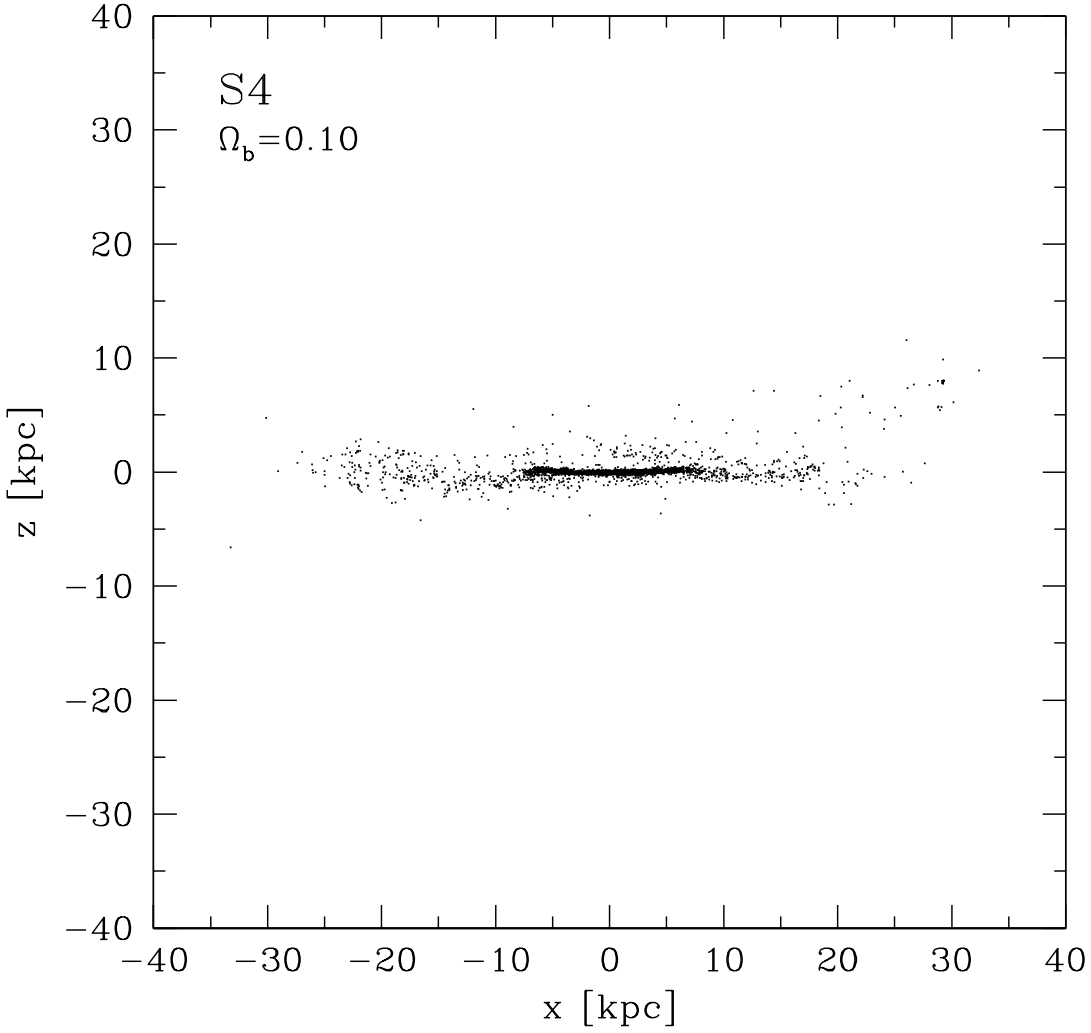

Fig. 14.— An edge-on view of the galaxy in Fig. 13.

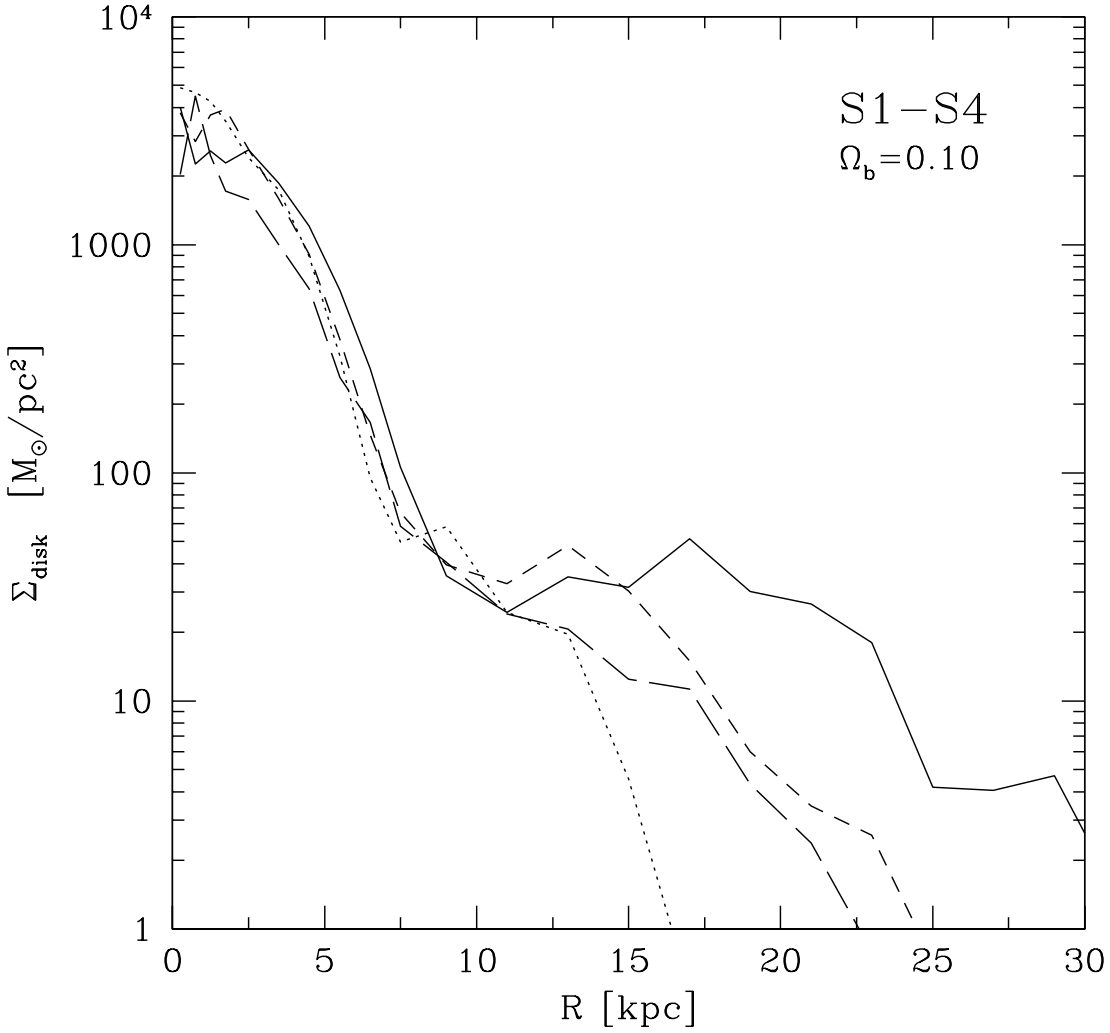

Fig. 15.— Azimuthally averaged disk surface density profiles of the final disk galaxies formed in the WDM2, MR simulations (with $\Omega_b = 0.10$ and UVX radiation field) of galaxies S1 (*long-dashed line*), S2 (*dotted line*), S3 (*short-dashed line*) and S4 (*solid line*).

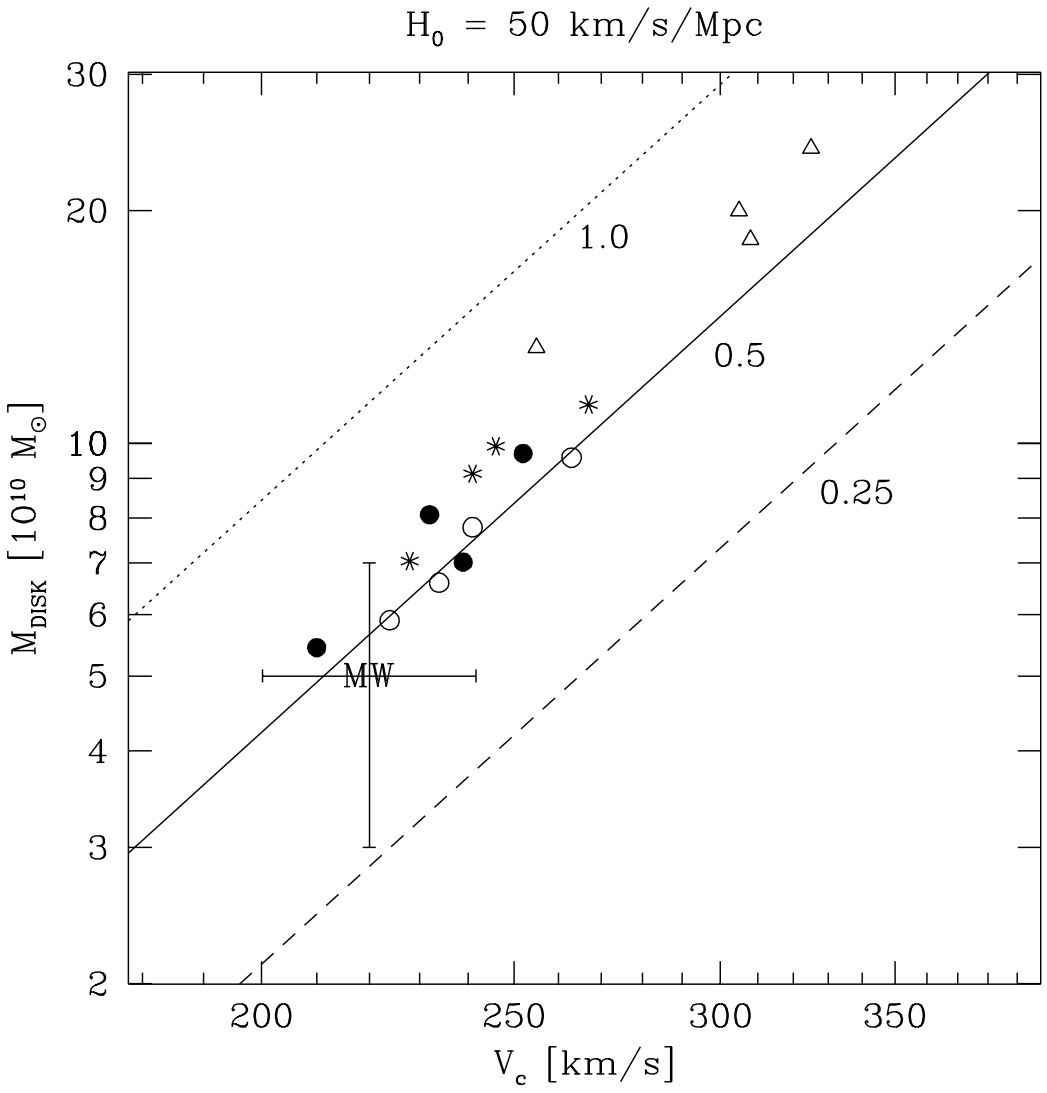

Fig. 16.— The mass vs. circular velocity "Tully-Fisher" relation for the final disks of our 16 WDM2 simulations - symbols used are the same as in Fig. 12. Also shown is the observed I-band TF relation of Giovanelli et al. converted to mass assuming $(M/L_I) = 0.25$ (*dashed line*), 0.5 (*solid line*) and 1.0 (*dotted line*). Finally, the symbol "MW" with errorbars shows the likely range of the total, baryonic mass and characteristic circular velocity of the Milky Way.

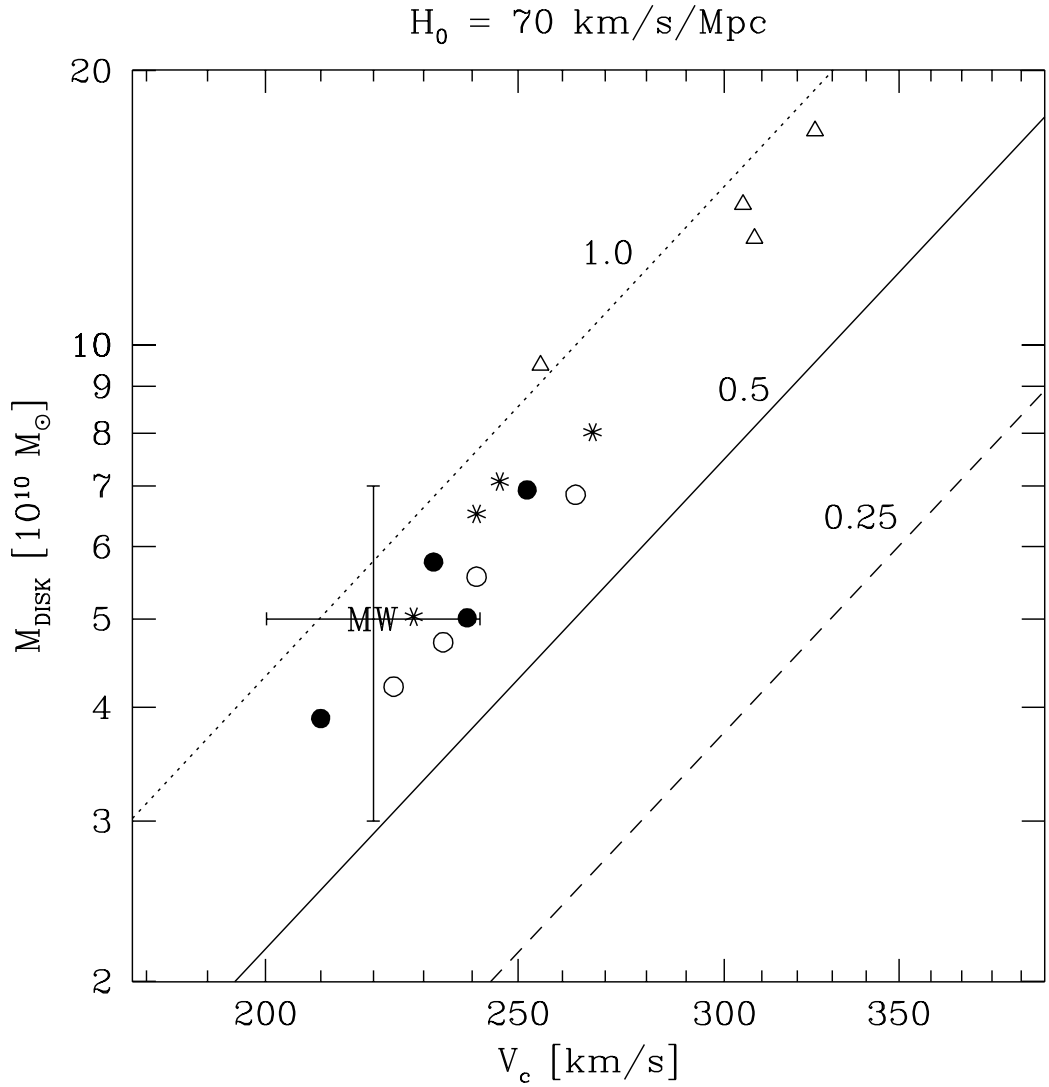

Fig. 17.— Same as Fig. 16, but for $H_0 = 70$ km/s/Mpc, rather than the 50 km/s/Mpc used in our simulations. The inferred absolute luminosities of observed galaxies scale as h^{-2} and we have assumed that the masses of simulated galaxies scale as h^{-1}.

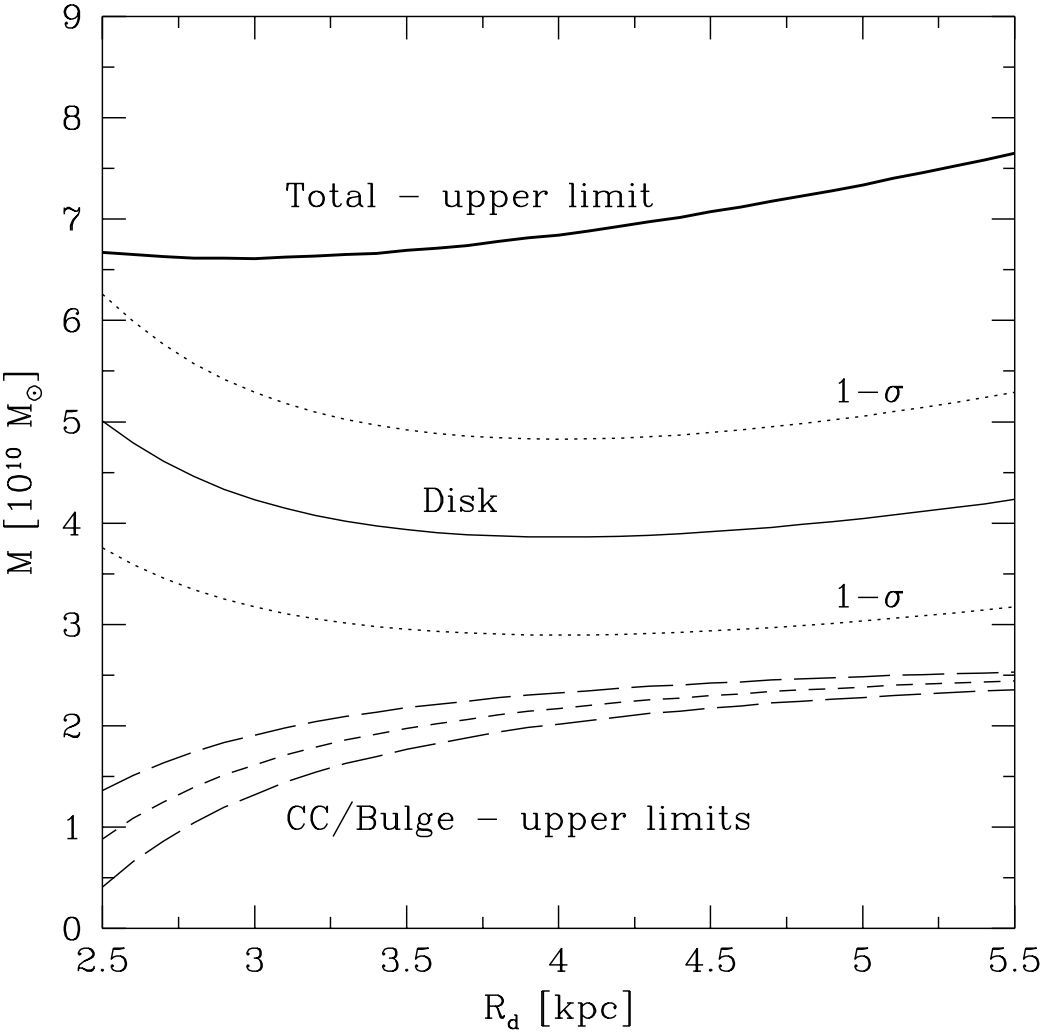

Fig. 18.— Baryonic mass of the Milky Way as a function of the disk scale-length R_d. The estimated mass of the disk is shown by the solid line and the 1-σ contours by the dotted lines. The upper limit to the mass of the central component/bulge is shown by the short-dashed line and lower and upper 1-σ contours by the long-dashed lines - see text for details. The 1-σ upper limit to the total, baryonic mass of the Milky Way is shown by the heavy, solid line.

Table 1: Parameters of the simulations

Run	Galaxy	DM type	Resolution	UVX field	Ω_b	$N_{\rm SPH}$	$N_{\rm DM}$
1	S4	WDM1	MR	yes	0.05	14736	7368
2	S4	WDM2	MR	yes	0.05	14700	7350
3	S4	WDM3	MR	yes	0.05	14848	7424
4	S1	WDM2	MR	yes	0.05	13700	6850
5	S2	WDM2	MR	yes	0.05	14142	7071
6	S3	WDM2	MR	yes	0.05	14404	7202
7	S1	WDM2	HR	yes	0.05	54689	54689
8	S2	WDM2	HR	yes	0.05	56386	56386
9	S3	WDM2	HR	yes	0.05	57723	57723
10	S4	WDM2	HR	yes	0.05	58739	58739
11	S1	WDM2	MR	no	0.05	13700	6850
12	S2	WDM2	MR	no	0.05	14142	7071
13	S3	WDM2	MR	no	0.05	14404	7202
14	S4	WDM2	MR	no	0.05	14700	7350
15	S1	WDM2	MR	yes	0.10	13700	6850
16	S2	WDM2	MR	yes	0.10	14142	7071
17	S3	WDM2	MR	yes	0.10	14404	7202
18	S4	WDM2	MR	yes	0.10	14700	7350

Table 2: Masses, sizes and velocities at $z = 0$

Run	M_{200} [10^{12} $M_\odot$]	r_{200} [kpc]	V_{200} [km s^{-1}]	N_{gas}	N_{DM}	M_{gas} [10^{10} $M_\odot$]	M_{DM} [10^{12} $M_\odot$]	N_{disk}	M_{disk} [10^{10} $M_\odot$]	M_{disk} [$\Omega_b M_{200}$]
1	3.25	382	191	5450	2850	15.59	3.10	3807	10.89	0.67
2	3.39	388	194	5663	2969	16.20	3.23	3392	9.70	0.57
3	2.42	346	173	4101	2098	11.82	2.30	1814	5.19	0.43
4	2.16	334	167	3590	1895	10.27	2.06	1903	5.44	0.50
5	2.37	344	172	4125	2074	11.80	2.25	2452	7.02	0.59
6	2.74	360	181	4812	2391	13.77	2.60	2824	8.08	0.59
7	2.18	334	167	15573	15206	11.14	2.07	8246	5.90	0.55
8	2.38	344	173	16955	16662	12.13	2.26	9224	6.60	0.55
9	2.68	358	179	19326	18686	13.82	2.54	10884	7.79	0.58
10	3.29	384	192	22602	23045	16.17	3.13	13392	9.70	0.58
11	2.15	332	167	3566	1822	10.20	2.05	2459	7.04	0.70
12	2.38	344	172	4429	2074	12.10	2.25	3191	9.13	0.77
13	2.78	362	182	4818	2426	13.78	2.64	3464	9.91	0.71
14	3.44	390	195	5801	3013	16.60	3.28	3922	11.22	0.66
15	2.16	332	167	3543	1892	20.27	1.95	2338	13.38	0.62
16	2.42	346	174	4357	2110	24.93	2.17	3203	18.33	0.76
17	2.83	364	183	4981	2475	28.50	2.55	3486	19.96	0.70
18	3.46	390	195	5945	3025	34.02	3.12	4205	24.06	0.69

Table 3: Circular velocities and specific angular momenta at $z = 0$

Run	V_c [km s^{-1}]	λ	j_{disk} [kpc km s^{-1}]	r_{inf} [kpc]
1	286	0.056	381	176
2	252	0.045	800	151
3	173	0.011	239	120
4	210	0.026	462	122
5	239	0.027	375	145
6	232	0.045	411	149
7	224	0.017	-	132
8	234	0.025	997	134
9	241	0.049	648	144
10	263	0.050	1276	150
11	228	0.018	637	166
12	241	0.018	623	199
13	246	0.046	724	201
14	267	0.052	866	178
15	255	0.020	1056	148
16	308	0.022	1000	201
17	305	0.045	1312	194
18	325	0.054	1990	186